Biochemistry and Chemical Biology
Structural Biology and Molecular Biophysics

Reviewed Preprint
v2 • June 18, 2025
Revised by authors

Reviewed Preprint
v1 • March 4, 2025

Polyphosphate Discriminates Protein Conformational Ensembles More Efficiently than DNA Promoting Diverse Assembly and Maturation Behaviors

Saloni Goyal, Divya Rajendran, Anup Kumar Mani, Athi N Naganathan

Department of Biotechnology, Bhupat & Jyoti Mehta School of Biosciences, Indian Institute of Technology Madras, Chennai, India

eLife Assessment

This manuscript offers **important** insights into how polyphosphate (polyP) influences protein phase separation differently from DNA. The authors present **compelling** evidence that polyP distinguishes among protein conformational ensembles, leading to divergent condensate maturation behaviors that include unfolding and polyproline II formation. In response to reviewer feedback, the authors addressed key concerns by incorporating charge-equivalent DNA controls and extending structural analysis to FruR variants, further reinforcing the polymer-specific effects of polyP. While some discrepancies between protein systems remain unresolved, the study enhances our understanding of how biopolymers influence protein assembly and conformational transitions.

https://doi.org/10.7554/eLife.105461.2.sa3

Abstract

Disordered proteins and domains often assemble into condensates with polyanionic nucleic acids, primarily via charge complementarity, regulating numerous cellular functions. However, the assembly mechanisms associated with the other abundant and ubiquitous, anionic, stress-response regulating polymer, polyphosphate (polyP), is less understood. Here, we employ the intrinsically disordered DNA binding domain (DBD) of cytidine repressor (CytR) from *E.coli* to study the nature of assembly processes with polyP and DNA. CytR forms metastable liquid-like condensates with polyP and DNA, while undergoing liquid-to-solid transition in the former and dissolving in the latter. On mutationally engineering the ensemble to exhibit more or less structure and dimensions than the WT, the assembly process with polyP is directed to either condensates with partial time-dependent dissolution or spontaneous aggregation, respectively. On the other hand, the CytR variants form *only* liquid-like but metastable droplets with DNA which dissolve within a few hours. Polyphosphate

induces large secondary-structure changes, with two of the mutants adopting polyproline II-like structures within droplets, while DNA has only minimal structural effects. Our findings reveal how polyphosphate can more efficiently discern conformational heterogeneity in the starting protein ensemble, its structure, and compactness, with broad implications in assembly mechanisms involving polyP and stress response in bacterial systems.

Introduction

Biomolecular condensates are mesoscale membrane-less structures that facilitate various cellular processes from stress response and signal transduction to RNA processing and chromatin organization.[1–5] Physically, condensates are formed by the demixing or phase separation of bio-macromolecules (i.e. proteins, DNA, RNA) into a polymer-rich or a condensed phase and a solvent-rich phase. The phase separation can be driven by homotypic or heterotypic interactions depending on the nature of demixing species, with a host of factors including the concentration and composition of constituent species, specific ions, ionic strength, temperature, and pH governing the transition.[6–8] Both folded and disordered regions of proteins can form condensates, with a lot more propensity and prevalence noted in the latter. Biomolecular condensates are also implicated in numerous diseases, and specifically in neurodegenerative disorders, with the condensates or sometimes the dilute phase proposed to seed the formation of aggregates and amyloids.[5,9–12]

Complex coacervation, wherein oppositely charged macromolecules condense and promote phase transition, is often observed in DNA- and RNA-binding domains that harbor excess positive charges to bind the anionic counterpart.[7,13–19] However, the role of inorganic polyphosphates (polyP), a series of phosphate units (Pi) linked together via phosphoanhydride bonds (**Figure 1A**), in condensate formation and maturation has been less explored. PolyP is a ubiquitous molecule that is produced under stress conditions like oxidative stress, heat shock, nutrition limitation, etc., in all organisms.[20–22] In fact, the polymer length of polyP and the concentration vary among different species ranging from few tens to thousands, reaching up to 50 mM in bacterial cells under stress conditions.[20] Apart from stress response, it has been implicated in numerous processes ranging from modulation of nucleoid structure to biofilm formation.[23–28] Intriguingly, polyP is able to act both as a chaperone[29] (assisting folding of proteins, preventing protein misfolding and inhibiting aggregation) and in promoting aggregation,[30,31] indicative of more complex underlying mechanisms[32,33] which could be protein-specific.

Based on the observations above, we pose this question: is polyphosphate more sensitive to the starting conformational ensemble than DNA leading to differential behaviors of promoting aggregation versus acting as a chaperone? If so, and given the poly-anionic nature, does it lead to aggregates or condensates or both? To answer these questions, one needs a system which is also a DBD to enable direct comparison. Second, the DBD should be mutationally tunable to populate native ensembles with different structure, compactness and helicity. Third, the charge composition and their sequence patterning should not be changed across the mutants, as this will naturally affect the binding to polyP. Here, we employ Cytidine repressor DBD (CytR DBD or CytR or CytR wildtype), an intrinsically disordered domain (**Figure 1B**, 1C) that adopts a folded conformation in the presence of DNA,[36] as a model system to answer these questions. Despite its disordered nature, mutations of different types and at different positions can be introduced into CytR to make it adopt a continuum of conformations, from highly disordered to globally ordered (i.e with a specific three-dimensional structure).[37–39] Specifically, the WT populates a minor excited state which is fully folded (~8-10%), but otherwise the native ensemble is disordered, with marginal helicity and a Stokes radius of 19.5 Å (green in **Figure 1D**, 1F).[37,40] One of the mutants we consider is the double mutant of CytR (A29V/A48M; DM) which displays the properties of a fully folded compact domain driven by the enhanced hydrophobicity of the side-chains at positions 29

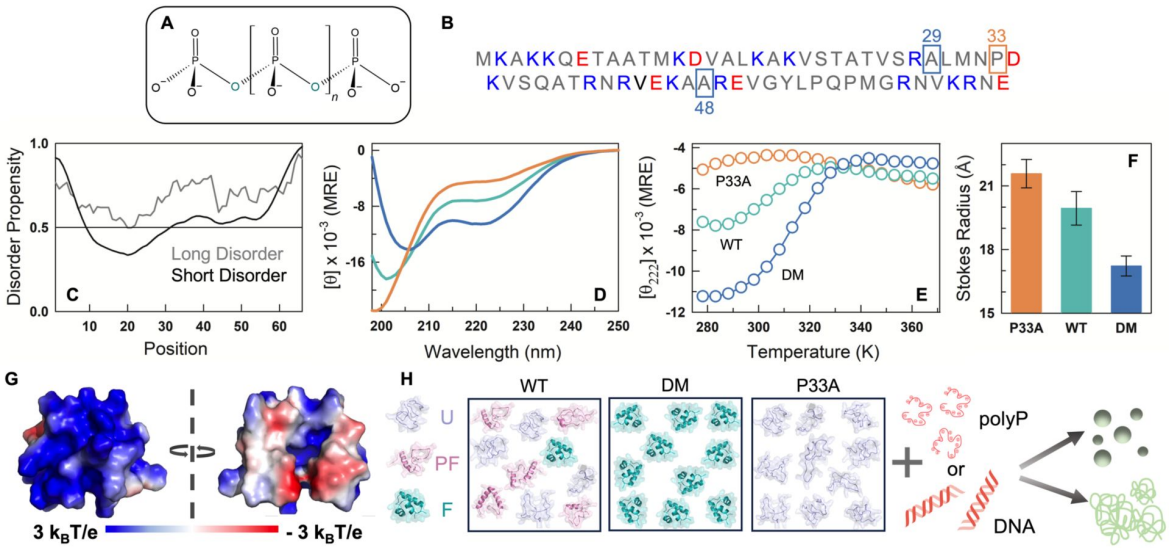

Figure 1

Conformational features of CytR WT and mutants.

(A) Molecular structure of polyP. (B) Amino acid sequence of CytR. Blue and red boxes indicate the positions of alanine and proline mutations in DM and P33A variants, respectively. (C) Disordered propensity of CytR predicted using IUPred3[34] with gray and black curves showing long and short disorder predictions, respectively. (D) Far-UV CD spectra of WT (green), DM (blue), and P33A (red) at 298 K in mean residue ellipticity (MRE) units of deg. cm^2 $dmol^{-1}$. (F) Thermal denaturation curves of CytR variants from far-UV CD experiments monitored at 222 nm and reported in MRE units. (F) Stokes Radius following the color code in panel E. (G) Electrostatic potential map[35] of CytR in its folded conformation displaying a large positive electrostatic potential. (H) The hypothesis tested in the current work. WT (left), DM (middle), and P33A (right) ensembles could potentially form condensates or aggregates in the presence of polyP or DNA, and which could also display differential time-dependent properties. U, PF, and F represent unfolded, partially folded and folded conformations, respectively.

and 48; these two mutations act synergistically to switch the ensemble from being disordered to fully ordered as shown earlier.[38] The DM therefore displays a higher helicity and lower Stokes radius of 17 Å, compared to the WT (blue in **Figure 1D**, 1F). The other mutant is P33A in which the minor folded state population is eliminated because of the enhanced flexibility of alanine in the place of proline.[37] The P33A mutant is nearly fully disordered as evidenced by the Stokes radius of 21.5 Å, and minimum helicity (red in **Figure 1D**, 1F).

In addition, because CytR has an excess charge of +9 and a large positive electrostatic potential in its folded conformation (**Figure 1G**), it binds non-specifically to DNA.[41,42] We therefore hypothesize that CytR should bind to any negatively charged polymer driven purely by electrostatic complementarity. In this work, we employ CytR WT and two mutants of CytR that exhibit diametrically opposing conformational preferences but identical charge composition and two anionic polymers (polyP and DNA), to understand the extent to which the starting ensemble (and hence the density of charges and stability or structure) dictates the nature of macromolecular assemblies and their maturation properties (**Figure 1H**). We find that the starting conformational ensemble is uniquely recognized by polyphosphate leading to diverse outcomes including metastable condensates, aggregates and time-dependent dissolution.

Methods

Purification of CytR DBD and mutants

The gene corresponding to the DNA binding domain of CytR(MKAKKQETAATMKDVALKAKVSTATVSRALMNPDKVSQATRNRVEKAAREVG YLPQPMGRNVKRNE) in the pTXB1 vector was transformed in to *E.coli* BL21 (DE3) cells and purified as described before.[41] Identical protocols were employed for purification of the DM and P33A variants. The Stokes radius was estimated as detailed in an earlier work.[39]

Time-dependent scattering (OD) and Thioflavin T (ThT) fluorescence measurements

Different concentrations of CytR WT were prepared by dissolving the lyophilized protein in 20 mM sodium phosphate, pH 7 (43 mM ionic strength) buffer. To generate the phase diagram, the scattering intensity (optical density) was recorded at 350 nm at protein concentrations of 5, 25, 55, 90, and 120 μM, and at different polyP concentrations of 3, 6, 11, 22, 41, and 100 μM. The measurements were acquired for 24 hours at 7-minute intervals in a microplate reader (Agilent BioTek Synergy H1) at 298 K. The sample volume in each well was 200 μl. Further studies employed 90 μM protein (WT and mutants) and 22 μM polyP, unless mentioned otherwise. For the time-dependent studies recording both scattering and fluorescence, a 5 μM ThT (Sigma-Aldrich) was also added to the protein and polyP mixture; the wells were also excited at 442 nm, and the fluorescence intensity recorded at an emission wavelength of 485 nm. Ionic strength dependent experiments were carried out at 20 mM sodium phosphate buffer, pH 7.0 (43 mM effective ionic strength) with the addition of NaCl for a final ionic strength values spanning 60 - 200 mM. The OD values are reported directly from the plate reader without correction for pathlength which is 5 mm in this experiment.

For the scattering measurements in the presence of DNA, a range of CytR WT concentrations (2 – 100 μM) were used, and measurements were acquired with 1 μM of 45-bp dsDNA (5’ TGGTGGGTAAATTTATGCAACGCATTTGCGTCATGGTGATGAGTA 3’). Further studies with DNA were done at 25 μM protein (WT and mutants) concentration.

NHS-rhodamine labeling

NHS-rhodamine (ThermoFisher Scientific, USA) was dissolved in DMSO, and protein was dissolved in conjugation buffer at pH 7.4 (as per manufacturer's protocol). The protein solution was added to 5X – 7X molar excess of dye and incubated at 25 °C for 2 hours at mild shaking conditions in dark. The excess dye was removed by desalting using a 26/10 HiPrep desalting column (Cytiva). The labeled protein was eluted in 20 mM sodium phosphate buffer at pH 7.

Flow chamber preparation for imaging experiments

Imaging experiments were done using 22 mm coverslips and glass slides (Blue Star, India). Coverslips and glass slides were kept in Piranha solution (3:1 v/v sulphuric acid and hydrogen peroxide) for 30 minutes and then washed thoroughly with MilliQ water. The slides and coverslips were then air-dried and wiped with absolute ethanol. Clean slides and coverslips were used to prepare flow chambers to observe the condensate formation. To prepare the flow chamber, the double-stick tape was sandwiched between the glass slide and coverslip. The chamber was then sealed from three sides to avoid sample leakage.

Fluorescence microscopy

The condensates were observed under 100X/1.45 NA oil immersion objective at room temperature using Olympus IX83 inverted fluorescence microscope. 10% of the labeled protein was mixed with unlabeled protein, and the sample was loaded into the flow chamber immediately after adding polyP/DNA. An anti-fading cocktail containing 20 µg/ml glucose oxidase, 1.4 µg/ml catalase, 20 mM glucose and 10 mM dithiothreitol was used to prevent photobleaching of the sample.[43] The sample was imaged at different time points under DIC and fluorescence mode using an appropriate fluorescence channel at 2048 x 2048 pixels (images for WT in the presence of polyP were acquired at 1024 x 1024 pixels) with 8-bit depth resolution. Images were analyzed using cellSens Dimensions Desktop (provided with the instrument) and ImageJ.[44]

Fluorescence recovery after photobleaching (FRAP)

For FRAP experiments, 10% and 5% of labeled protein were used for polyP and DNA studies, respectively. Anti-fading cocktail was added to the protein sample to prevent the passive photobleaching. The samples were loaded into the flow chamber at different time points (0, 30, and 60 min), and the experiment was performed in an Olympus Fluoview FV3000 confocal microscope with a 100X/1.45 NA oil immersion objective. A 561 nm laser was used to visualize and bleach (with 100% laser power) the condensates at the center. Fluorescence intensity was acquired for five different regions of interest (ROIs) with the same diameter; ROI-1 for the actual bleaching region, ROI-2 for the neighboring condensate for passive bleaching correction and ROI-3,4 and 5 outside the condensates to record background intensity for background correction. The images were acquired at 1024 x 1024 pixels with 12-bit resolution. Data was processed using cellSens Dimensions Desktop software and MATLAB. The raw data was corrected using the following equation[45]

$$I(n) = \frac{I(t) - I(b)}{I_c / I_{c_o}}$$

where, $I(t)$ is the fluorescence intensity at time t, $I(b)$ is the average of background intensity for ROI-3,4, and 5, I_c is the fluorescence intensity of ROI-2 after photobleaching and I_{co} is the fluorescence intensity before photobleaching. The data was normalized (I) using:

$$I = \frac{I_n - I_{n_{min}}}{I_{n_o}}$$

where I_n is corrected fluorescence intensity at time t and I_{no} is the intensity before bleaching and $I_{n_{min}}$ is the minimum intensity. The average of corrected and normalized fluorescence intensity from different experiments was taken, and the data was plotted as a function of time.

Circular dichroism (CD)

Far-UV CD spectra were recorded at protein concentrations 55 μM and 25 μM immediately after the addition of 22 μM polyP and 1 μM DNA, respectively. The spectra were acquired as a function of time for 4 hours at an interval of 15 minutes in the wavelength range of 250-200 nm at 298 K with a scanning speed of 10 nm/min in a Jasco J-815 spectropolarimeter. The mean helical content for the different CytR variants is estimated by taking the ratio between the signal at 222 nm with that expected of a 100% helical protein (−40,000 MRE units of deg. cm^2 $dmol^{-1}$).

Fourier-transform infrared (FTIR) spectroscopy

FTIR scans were performed using a Perkin Elmer Spectrum Two Spectrometer equipped with a DTGS detector in the attenuated total reflectance (ATR) mode. 5 μl of protein sample was added to the diamond crystal, and the spectrum was acquired in the range of 4000-400 cm^{-1} using an average of 50 scans at a resolution of 4 cm^{-1}. Baseline correction was done with MilliQ water to minimize the interference due to H_2O before spectral acquisition.

Results and Discussion

CytR WT and DM form condensates with polyphosphate while P33A aggregates

Inorganic $polyP_{45}$, i.e. polyphosphate with 45 Pi units and with a net-charge of -47, is employed in our studies and is referred to as polyP in the text below. We explored a range of solution conditions involving two-component mixtures of WT and polyP ([polyP] of 3 - 100 μM and [WT] of 5 – 125 μM at 20 mM phosphate buffer, pH 7 and 298 K) to map the phase diagram (**Figure 2A**). Solutions containing [WT]>25 μM and [polyP]>10 μM consistently showed higher turbidity (turbidity at 350 nm). We therefore chose [polyP] of 22 μM for further experiments. DIC (differential interference contrast) microscopy reveals droplet-shaped condensates with a diameter of ~1-4 microns on average (**Figure 2B**; also *vide infra*), which is also confirmed by fluorescence microscopy of NHS-rhodamine-labeled protein (**Figure 2C**). The number of droplets increase with increasing [WT] in the range between 25 – 90 μM consistent with OD measurements (**Figure 2D**). These observations establish that the WT CytR undergoes phase-separation into condensates with polyP, and that turbidity can be employed as a reasonable proxy for phase separation in this system.

Given that CytR carries a large excess positive charge (+9) and polyP is an anionic polymer with no structural preference (unlike DNA), the interaction and the resultant assembly process is expected to be driven by non-specific electrostatic interactions. To test this, we use a [WT]:[polyP] of 90:22 μM and measure OD as a function of ionic strength at pH 7. The OD is observed to be independent of ionic strength till ~80 mM following which it linearly decreases with near-zero turbidity at 200 mM (**Figure 2E**). Under physiological ionic strength conditions of 150-160 mM, the OD value is still ~0.6 and with droplets evident in fluorescence microscopy (**Figure S1**).

The double mutant (DM) which is folded and compact, also undergoes spontaneous phase separation at the same concentrations as the WT when mixed with polyP, while the P33A mutant aggregates on addition of polyP (**Figure 2F**, 2G). The fluorescence of the NHS-rhodamine-labeled WT and DM recover on photobleaching highlighting the liquid-like nature of the condensates (**Figure 2H**). Specifically, the WT displays a maximal recovery of ~92% at 90 seconds (recovery

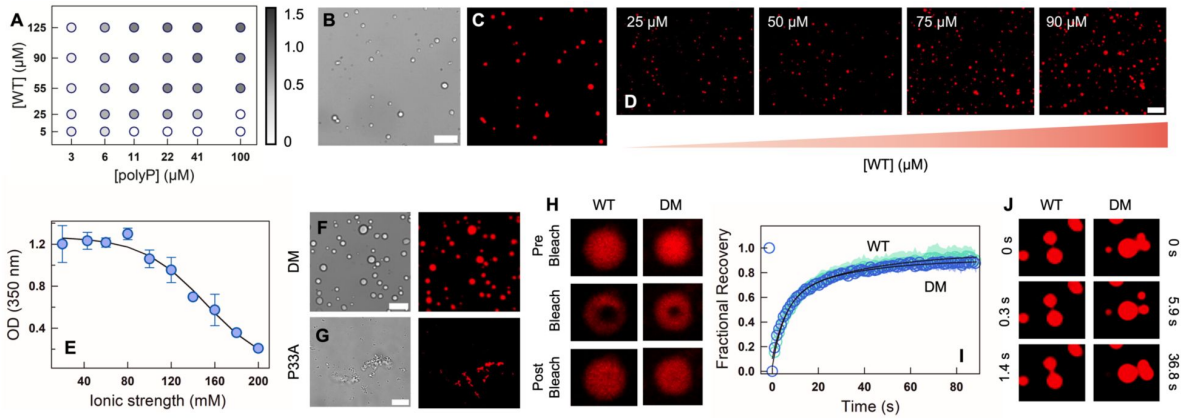

Figure 2

CytR undergoes phase separation with polyP *in vitro*.

(A) Phase diagram illustrating the phase separation of WT at different protein and polyP concentrations. Empty circles represent no phase separation, and filled circles represent the extent of phase separation following the color bar which indicates the OD (turbidity) at 350 nm. (B, C) Representative DIC (B) and fluorescence (C) microscopy images of WT showing condensate formation in the presence of polyP. (D) Fluorescence microscopy images of NHS-rhodamine labeled WT at different protein concentrations in the presence of 22 μM PolyP. The scale bar is 10 μm. (E) Ionic strength dependence of turbidity at fixed WT (90 μM) and polyP (22 μM) concentrations. The error bar indicates the spread from experimental replicates (N=2) . (F, G) DIC (left) and Fluorescence (right) microscopy images of NHS-rhodamine labeled DM (F) and P33A (G) in the presence of polyP. The scale bar is 10 μm. (H) Representative fluorescence microscopy images of condensates during FRAP on WT (left) and DM (right) immediately after polyP addition. (I) FRAP recovery curves at 0 h for DM (blue) and WT (green). The data represents an average of five experiments (N=5) and the errors (shaded areas) are smaller than the size of the circles. (J) Time-lapse fluorescence images showing a dripping event for the WT (left column) and fission-fusion events for DM (right column).

half-time, $t_{1/2}$ = 6.0 ± 2.5 seconds), and the DM recovers to ~87% ($t_{1/2}$ = 5.2 ± 1.3 seconds) (**Figure 2I**). We also observe multiple coalescence and de-coalescence events in both the proteins at the earliest times (**Figure 2J**, Supporting Movies S1 and S2).

Taken together, the fully unfolded variant of CytR (P33A) forms aggregates and the variants with more 'folded-like' states undergo phase separation with polyP. These results indicate that charge-composition and patterning alone do not determine the phase separation tendencies in this system. They underscore the importance of the starting ensemble, and potentially the population of partially structured substates, in determining the nature of assembly process observed.

Maturation of polyphosphate-induced assemblies

We carried out time dependent studies in the presence of thioflavin T (ThT) enabling simultaneous measurement of OD and fluorescence in the same sample. The OD of WT-polyP mixtures show a strong time dependence with the OD decreasing from 1.2 to less than 0.9 in the first 10 minutes, but with little increase in ThT fluorescence (left panel in **Figure 3A**). However, the ThT fluorescence starts to increase in a sigmoidal fashion from 20 minutes. The OD, on the other hand, drops to a value of 0.75 at ~30 minutes following which it increases and stabilizes at a value of ~1. The WT-polyP mixture therefore forms condensates and matures into aggregates within 3 hours which is directly observable in microscopy images (**Figure 3B**), mirroring reports in numerous other systems that undergo droplet formation followed by a liquid-to-solid phase transition.[46–50] Control experiments with protein alone did not reveal any changes in turbidity or aggregation in the entire 24-hour duration (**Figure S2**), pointing to a process entirely driven by polyP-protein interactions.

The OD of the DM-polyP mixture exhibits a similar decrease in OD starting from a value of ~1, but this trend extends beyond 3 hours, with the OD dropping to a value of ~0.1 at the longest time points (middle panel in **Figure 3A**). We do observe a marginal increase in ThT fluorescence after 2 hours, but the increase is not as significant as the WT. These observations point to a scenario wherein the DM forms condensates to start with, but which slowly dissolve with time (**Figure 3B**). On the other hand, the P33A mutant forms only aggregates as evidenced by the high OD and high ThT fluorescence across all time-points in the 24-hour observation window (right panel in **Figure 3A**, 3B). FRAP experiments follow the trends reported in OD-fluorescence measurements. In the WT, the recovery amplitude decreases from 0.92±0.11 at the zeroth minute to just 0.43±0.04 at 60 minutes (**Figure 3C**, 3D). The FRAP $t_{1/2}$, however, drops to shorter times at t = 60 minutes indicating that there is small sub-set of dynamic molecules (i.e. a small percentage of mobile fraction) contributing to the rapid recovery (**Figure 3E**). Alternately, the DM-polyP condensates recover near fully even at the first hour, with the recovery time slowing time by a factor of 2 (**Figure 3F**-**3H**).

We further quantified the dimensions of the droplets from the microscopy images at three different time-points: 0, 30 and 60 minutes. At t = 0 and for the WT-polyP condensates, the mean droplet dimensions are of the order of 2.7 microns, but with a heavy right tail spanning nearly 8 microns. This tail is diminished at t = 30 minutes, reducing the overall dimensions of droplets (~2.4 microns) and their number (smaller area under the curve in **Figure 3I**). The DM displays a behavior which is the exact opposite (**Figure 3J**): at t = 0 the mean dimensions of the condensates are 2.1 microns with no heavy right tail; larger droplets appear at t = 30 minutes contributing to the appearance of the heavy right tail and with the mean droplet size increasing to 3.3 microns. At longer times (t = 60 minutes), the number of droplets reduce and so do their mean dimensions as a result of dissolution.

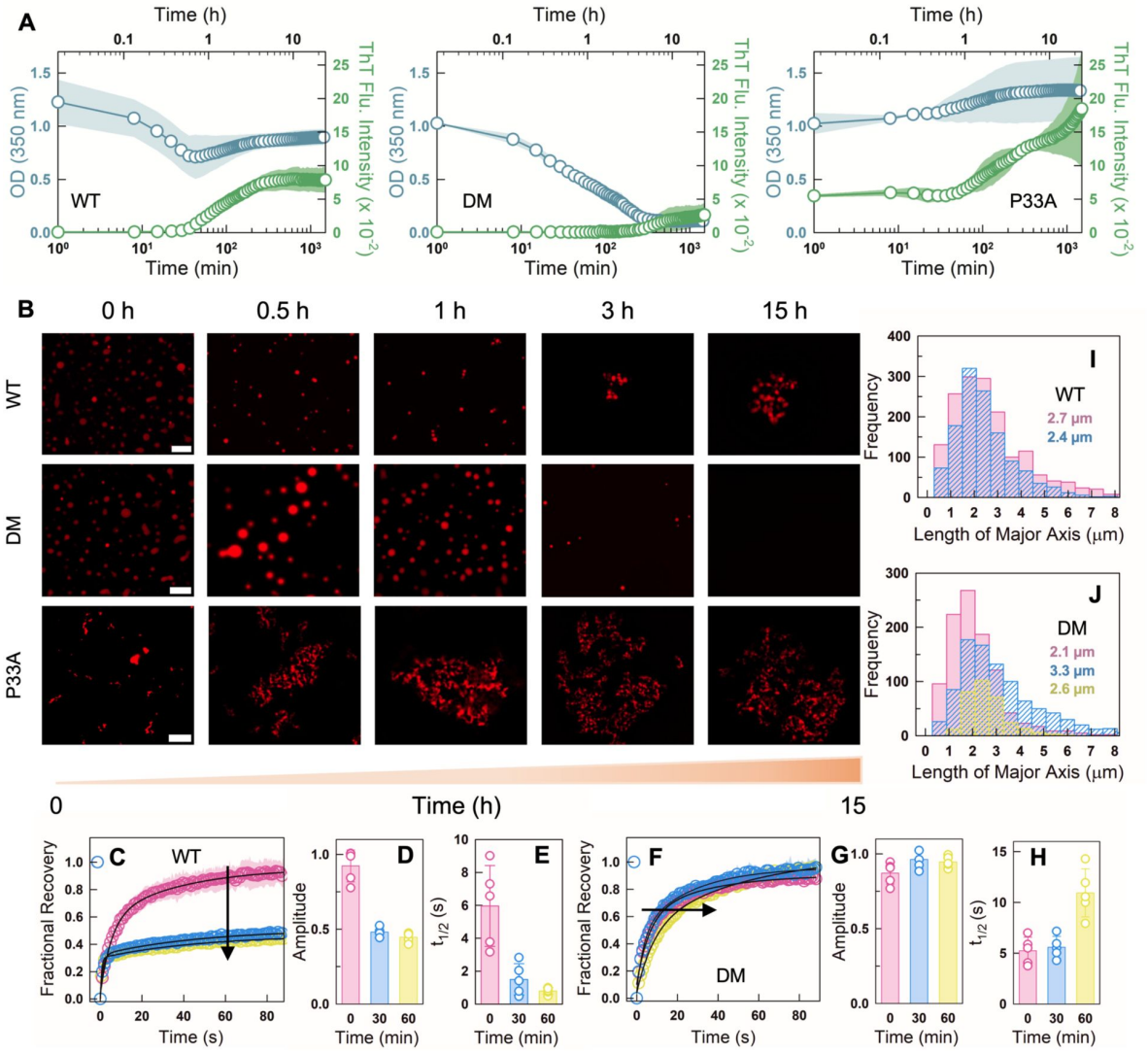

Figure 3

Time-dependence of polyP-induced assemblies.

(A) Turbidity (blue circles and left y-axis) and Thioflavin T fluorescence intensity (green circles and right y-axis) time dependence for 90 μM WT (left panel), DM (middle panel), and P33A (right panel) in the presence of 22 μM polyP. The average from N = 2 experiments (circles) and the spread in the respective data (shaded region) are shown. (B) Representative fluorescence images of NHS-rhodamine labeled WT (top panel), DM (middle panel) and P33A (bottom panel) in the presence of polyP at different time points. The scale bar is 10 μm. (C-H) FRAP experiments for WT (panels C-E) and DM (panels F-H) in the presence of polyP at different time points - 0 min (pink), 30 min (blue), and 60 min (yellow) – and from five droplets (N = 5) and plotted as mean ± s.d. (C, F) The FRAP recovery curves of NHS-rhodamine labeled WT (panel C) and DM (panel F). The experimental errors (shaded areas) are also shown. (D, G) Recovery amplitudes or extents from FRAP experiments on the WT (panel D) and DM (panel G) at different time points. WT shows less recovery with time, indicating a liquid-to-solid transition, while the DM recovers fully. (E, H) FRAP recovery half-times for the WT (panel E) and DM (panel H) at the indicated time points. (I, J) Droplet size-distribution of WT (panel I) and DM (panel J) at different time points following the same color code in panels C-H. The numbers within the plot represent the mean droplet dimensions at the corresponding time points.

Structural changes within the condensates span over three hours

The differential behavior of the three variants raise questions on the nature of structural changes upon condensate formation and maturation. The WT CD spectrum in the dilute phase (i.e. in the absence of polyP) is characterized by minima at 202 and 222 nm with ~17% of residual helical content (**Figure 1D**). Upon formation of condensates, the spectral shape shifts substantially to one with a minimum at 230 nm and with no spectral features at wavelength <215 nm (**Figure 4A**), demonstrating that the WT adopts a non-helical and potentially an unfolded conformation in the condensed phase at initial times. The spectrum of DM is more representative of a folded protein with minima at both 208 and 222 nm (**Figure 1D**), and with the signal at 222 nm indicative of a protein with nearly 30% helical content. On mixing with polyP, the spectral shift resembles that of the WT (**Figure 4B**), again indicative of a structural change in the condensed phase. The P33A mutant which is more unfolded (helicity ~10%), however, exhibits a more intense spectrum with a minimum 225 nm which is representative of β-sheet like structures (**Figure 4C**; see below). These differences are more evident when the signal at 222 nm are plotted as a function of time: the WT and P33A mutant exhibit a trend quite different from that of the DM, with the latter acquiring structure with time despite unfolding on adding polyP (**Figure 4D**).

Since the spectra measured with polyP are an effective average of structural signatures from both the condensed- and dilute-phases and of different secondary-structure types, the spectral shapes cannot be directly interpreted. To extract structural signatures and the associated trends, we perform a global singular value decomposition (SVD) of the spectral time series of the three variants. The first two components contribute 92% of the overall signal change (**Figure 4E**). Of this, the first component is the spectrum of an α-helix with clear minimum at 222 nm and another at 208 nm, and accounts for 71% of the signal change. The amplitude of this component decreases with time in the WT and P33A variant, implying that helical conformations are less favored in their assemblies; this feature also signals the population of an alternate structural form which is observable in the second component (**Figure 4F**). In the DM, the amplitude of the helical component increases with time as expected when the droplet dissolves due to preferential transport into the dilute phase. However, the helical content recovers to just ~15% at 4 hours (**Figure 4F**), conceivably due to non-specific interaction with polyP resulting in partially structured states or due to a small fraction of oligomers.

The second component, accounting for 21% of the signal change, bears the features of polyproline II structures in unfolded conformations[51] with a maximum at 231 nm and a minimum at 207 nm (**Figure 4E**). There is a marginal increase in the amplitude of this component in the WT in the first hour following which it stabilizes (**Figure 4G**). The amplitude of this component increases in the DM continuously even at 4 hours indicating a tussle between the helical and polyproline II-like structures (**Figure 4G**). Since the droplets are fully dissolved at 4 hours and by which time the ThT fluorescence starts to marginally increase, it is likely that smaller-sized aggregates (as the contribution of this component is only 20% of the overall change) coexist with folded, and partially structured helical conformations in the DM-polyP mixtures at longer times. In the P33A variant, the amplitude of second component has a negative sign and when multiplied with the second component (required for reconstructing the original spectra) points to a strong contribution from β-turn or polyproline I conformations, mixed with β-sheet.[52] This is further confirmed by FTIR spectroscopy on P33A wherein a strong absorbance band is evident in the wavenumbers 1610 – 1630 cm^{-1}, which is absent in both the WT and DM at t = 0 (**Figure 4H**-**4J**). At t = 60 minutes, the relative intensity of this band increases in the WT and P33A, while no change in spectral shape is evident for the DM.

In summary, we find that both the WT and the DM 'unfold' on forming condensates with polyP, with polyproline II-rich structures observed at longer times (~1-2 hours) in both the mixtures. The condensates thus formed are metastable, either undergoing a liquid-to-solid transition as in the

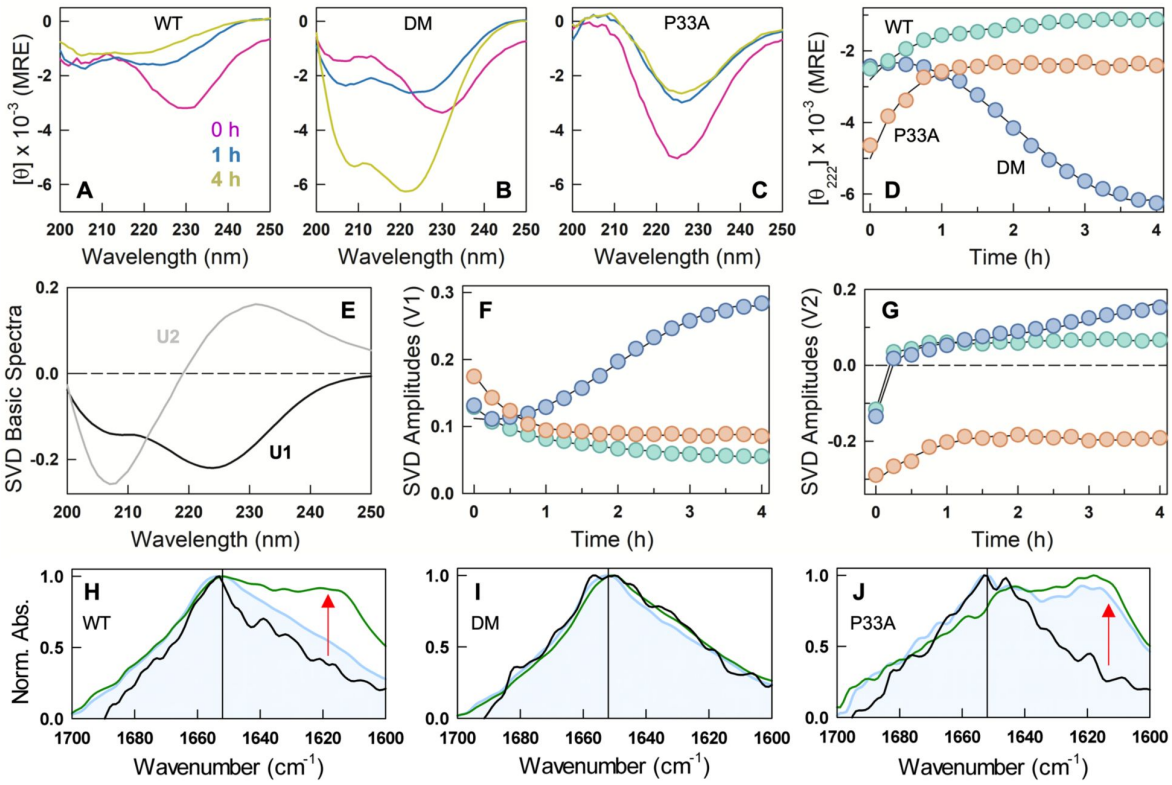

Figure 4

Structural changes in polyP-induced assemblies.

(A-C) Far-UV CD spectra of 55 μM WT (A), DM (B), and P33A (C) at different time points - 0 hour (pink), 1 hour (blue), and 4 hours (yellow) - after the addition of 22 μM polyP at 298 K and displayed in mean residue ellipticity (MRE) units of deg. cm^2 $dmol^{-1}$. (D) Time dependence of the signal at 222 nm for the variants studied. Note the clear secondary-structure acquisition in the DM with time. (E) Basis spectra from a global singular value decomposition (SVD) of time-wavelength far-UV CD data. The first and second components are shown in black and gray, respectively. (F, G) Amplitudes of first (F) and second (G) spectra as a function of time for CytR variants following the color code in panel D. (H-J) FTIR spectra for WT (H), DM (I), and P33A (J) showing normalized absorbance recorded at the wavenumber range of 1700 – 1600 cm^{-1}. Black curves represent the FTIR spectra of protein in the absence of polyP. The blue and green curves are the FTIR spectra of protein after the addition of polyP at 0 min and 60 min, respectively. Red arrows indicate the change in peak intensity after the addition of polyP, showing beta-sheet-like conformation in WT and P33A between 1610-1630 cm^{-1}. The vertical black line is at 1652 cm^{-1}, the amide I frequency indicative of helical structure.

WT or partially dissolving with time as in the DM. At the 4-hour time point, however, the DM acquires helical character due to the partial dissolution of the condensates while the WT forms only aggregates. The starting ensemble thus determines the extent of metastability and the maturation of condensates, and not just the nature of assemblies formed.

DNA is insensitive to the starting conformational ensembles

DNA is the primary anionic polymer bound by CytR, albeit without sequence preference and involving a distribution of binding free energies.[41] We find that CytR WT also forms condensates with just 1 μM of double-stranded DNA in a concentration-dependent manner at 20 mM phosphate buffer, pH 7 (**Figure 5A**, 5B). The droplets are liquid-like displaying coalescence behavior (**Figure 5C**), recovering fully on photobleaching in a few seconds and with a FRAP $t_{1/2}$of 5.5 ± 0.7 seconds (green in **Figure 5D**, 5E), comparable to the droplets formed in the presence of polyP. Both the DM and the P33A variants form phase-separated condensates with DNA (**Figure 5F**, **5G**), unlike aggregated assemblies observed with polyP-P33A droplets (**Figure 2G**).

The time-dependent properties of the condensates with DNA again differ from those of polyP: the condensates dissolve within 90 minutes in both the WT and DM (**Figure 5H**, 5I), while taking nearly 3 hours for the P33A variant (**Figure S3**). Numerous droplets with a mean size of 1.6 μm form within the first few minutes (**Figure 5J**), which coalesce to form larger droplets of size 2-3 μM, following which they dissolve. The FRAP $t_{1/2}$increases by a factor of two at 60 minutes compared to the initial time point (**Figure 5K**), and a very slow phase is also observed at 60 minutes (**Figure S4A**), indicating ~20% immobile fraction. We find that OD is less sensitive to droplet formation with DNA, as we do observe few droplets even at 3 hours, a timepoint at which the OD is effectively zero (**Figure S3**). Both the DM and P33A mutants recover fully (amplitudes ~1) and with similar half-times compared to the WT at 60 minutes (**Figure S4**). To rule out the possibility of concentration differences (22 μM for polyP and 1 μM for DNA) contributing to the observed diverse behavior across the two anionic polymers, we carried out a set of control experiments at 11.2 μM DNA, a concentration at which the number of negative charges are equivalent to that of 22 μM polyP. However, the trends were identical to that observed at lower DNA concentration (**Figure S5**), further underscoring that the differences in chemical and conformational properties of the anionic polymers contribute to the diverse assembly behaviors.

None of the three proteins 'unfold' in the DNA-driven condensates; there is a marginal reduction (i.e. the signal becomes less negative) in the far-UV CD signal at t = 0 following which it quickly recovers to reach a value near that of the CD signal in the absence of DNA (**Figure 5L**-**5M**). The absence of large structural change or ageing into an aggregate with time is also evident in FTIR spectra which do not change significantly (**Figure S6**). The WT, however, does display 50% less negative signal at ~202-204 nm which shifts to longer wavelength after the first hour (blue and green spectra in **Figure 5L**), indicating helical structure acquisition and mirroring earlier reports.[36,37] At higher DNA concentrations as used in the current study, this structural shift appears to be offset by unfolding in other regions likely through non-specific interactions. This leads to little signal change at 222 nm – note that this shift is not observable in the two mutants – and thus requiring detailed atomic-level studies to discern the subtle structural modulations induced by DNA at longer times.

To further test the lack of sensitivity of DNA to the starting conformational ensemble, we carried out a similar time-dependent experiment with polyP and DNA, but with the folded DBD of FruR (fructose repressor; **Figure 6A**) and the molten-globular variant Y19A FruR.[53] PolyP spontaneously induces aggregation in FruR, while the molten-globular variant forms condensates but only at the earliest times (**Figure 6B**, **6C**, **6D**). The intensity of ThT fluorescence protein-polyP mixture increases with time indicating that polyP induces a time-dependent enhanced aggregation of FruR, while the FruR Y19A-polyP mixture undergoes a rapid liquid-to-solid transition within the first 20 minutes (**Figure S7**). As with the CytR WT, the change in turbidity

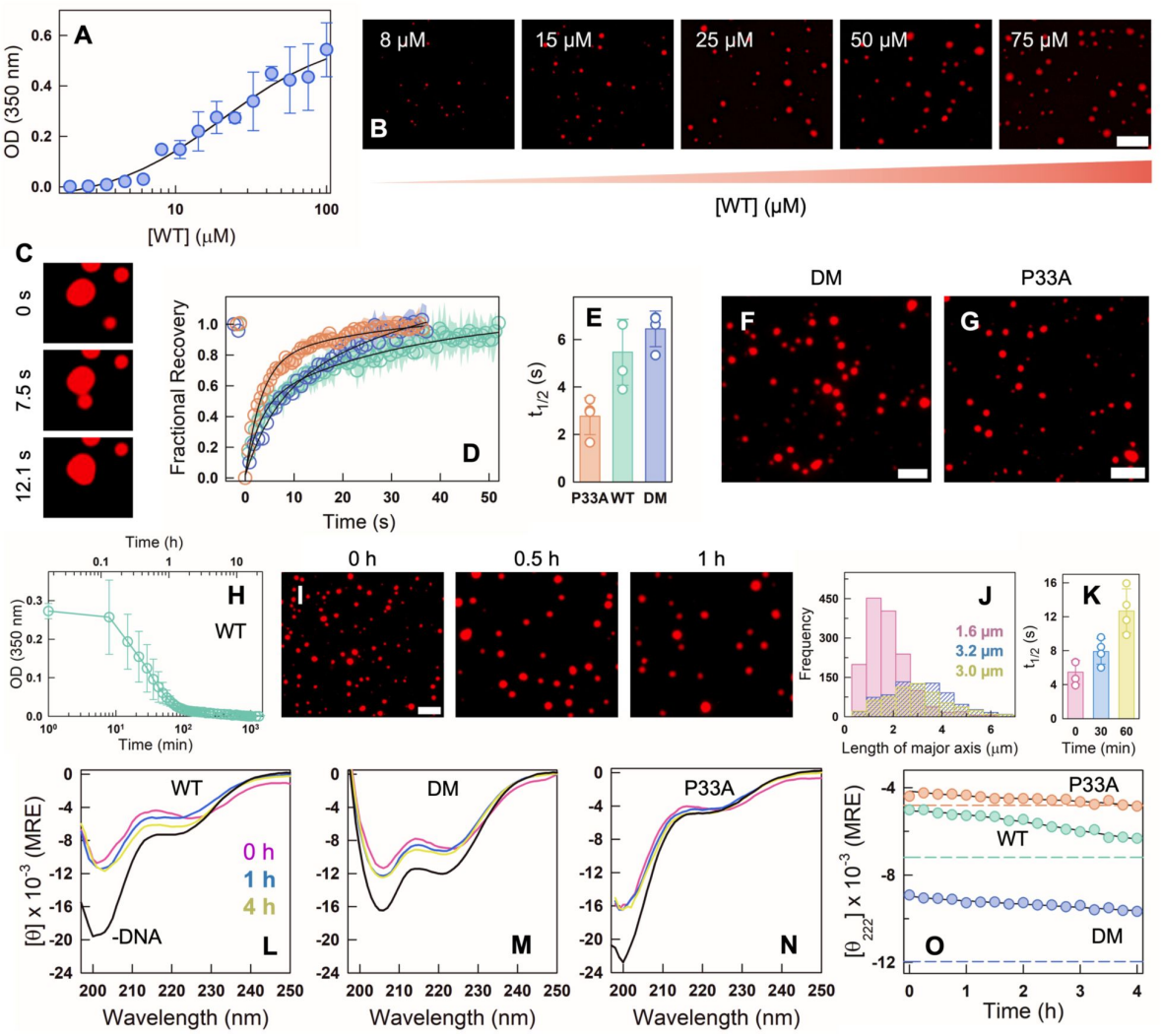

Figure 5

DNA induces metastable condensates that dissolve with time.

(A) Changes in turbidity in solutions containing increasing concentrations of the WT and a fixed 1 μM concentration 45-bp specific DNA. The data is the mean from N=2 experiments, and the error bar represents the spread. (B) Fluorescence microscopy images of NHS-rhodamine labeled WT at different concentrations with 1 μM DNA. The scale bar is 10 μm. (C) Representative time-lapse images of WT showing a fusion event. (D) FRAP recovery curves of NHS-rhodamine-labeled CytR WT (green), DM (blue), and P33A (red). The data represents average from N=4 experiments. The experimental errors are shown as shaded areas. (E) Recovery half-times for the CytR variants at the earliest time points (0 minutes). P33A shows the fastest recovery, followed by WT and DM. (F, G) Fluorescence microscopy images of 25 μM DM (F) and P33A (G) in the presence of 1 μM 45 bp DNA. The scale bar is 10 μm. (H) Turbidity of 25 μM WT with 1 μM DNA as a function of time. Data (circles) are from N = 2 experiments and the error bar indicates the spread. (I) Fluorescence microscopy images of NHS-rhodamine labeled WT with DNA at different time points. The scale bar is 10 μm. (J) Droplet size distribution curve for WT in the presence of DNA at different time points - 0 min (pink), 30 min (blue), and 60 min (yellow). Numbers within the plot represent the mean droplet dimensions at the corresponding time points. (K) Recovery half-times from FRAP experiment on WT with DNA at different time points for N=4 experiments following the color code for panel J. (L-N) Far-UV CD spectra of 25 μM WT (left), DM (middle), and P33A (right) at different time points - 0 hour (pink), 1 hour (blue), and 4 hours (yellow) - following the addition of 1 μM 45 bp DNA at 298 K. Black curve is the protein spectra in the absence of DNA. The data is reported in mean residue ellipticity (MRE) units of deg. cm^2 $dmol^{-1}$. (O) Time-dependent changes in far-UV CD signal at 222 nm for the CytR WT (green), DM (blue), and P33A (red). Dashed lines show MRE signal at 222 nm for the corresponding proteins in absence of DNA.

on aggregation happens earlier than the increase in ThT fluorescence (**Figure 6C**). In the presence of DNA, however, both the folded and the molten-globular variants display no change in turbidity with time (**Figure 6E**, **6F**).

Conclusions

Phase separation of disordered CytR with the anionic polyphosphate is quite robust to solution conditions. However, when the native ensemble is perturbed via mutations to result in more order (DM) or less order (P33A) relative to the WT, polyP induces either phase separation or aggregation, respectively (**Figure 2**). The time-dependent behavior is markedly diverse with liquid-to-solid transition, partial dissolution and enhanced aggregation in CytR, DM and P33A, respectively (**Figure 3**). The trends are consistent across the different experimental protocols employed including turbidity-fluorescence experiments, fluorescence microscopy, far-UV CD and FTIR (**Figure 2**-**4**). On the other hand, DNA forms only metastable condensates that dissolve with time, despite different degrees of structural order in the native ensemble of CytR variants (**Figure 5**). To further prove that polyP interacts differently with ensembles, we performed experiments on the molten-globular variant of FruR (Y19A mutant) and the folded wild-type protein; we see two different behaviors with the WT aggregating and the mutant undergoing a liquid-to-solid transition with polyP, while DNA does not form either aggregates or droplets (**Figure 6**).

The driving force for the different assembly processes is expected to have a strong contribution from the strength of intermolecular charge-charge interactions, the relative entropic penalty for inducing a conformational change in polyP versus that in the protein, release of counterions and restructuring of water. The balance between these different enthalpic-entropic terms results in condensates being more kinetically accessible phase but which are inherently metastable (as in the CytR WT, DM and FruR Y19A), as a strong time dependence is visibly observable even in the first few minutes. With time, they access the globally stable phase which is either the partially dissolved condensate or the more aggregated phase, conditions at which the chemical potential of the different constituent molecules equalize across the phases. Detailed molecular simulations that capture the relative experimental trends observed across the mutants are required to extract the contributions of each of the energetic and entropic terms.

Our observations establish that polyP is more sensitive to the conformational features of proteins than DNA, thereby contributing to the diverse outcomes. PolyP is expected to be highly flexible owing to its relatively simple chemical structure with only phosphoanhydride bonds that link adjacent units which are highly polar, while DNA has bulkier sugar and the apolar bases that limit its flexibility. It is therefore possible that polyP, owing to its flexibility, is able to wrap around the protein surface or even induce structural changes in proteins in a distinct manner depending on the nature of the starting ensemble. Strong evidence for the latter comes from our far-UV CD studies wherein we find that the helical signature of the CytR variants is fully lost on adding polyP (**Figure 4**). Our results are consistent with previous observations of structural changes and 'unfolding' of proteins within condensates.[54–57] We additionally show that polyproline-II-like conformations are more probable within condensates formed by the CytR WT and the DM (**Figure 4**). One other observation that stands out is that the ThT fluorescence increases upon aggregation at a later time point than the changes in OD that happens earlier in both the CytR WT and DM. In other words, dissolution of the droplet is likely happens even in the WT until about 30 minutes (the number of larger droplets also reduce in frequency; **Figure 3I**) following which it aggregates.

The large charge density associated with polyphosphates and their natural abundance makes them prime candidates for inducing phase separation[58] through complex coacervation with proteins rich in basic amino acids. In fact, most DBDs which are typically associated with transcription factors are rich in basic amino acids. This opens up a fascinating possibility where polyP and DNA could compete with transcription factors or work together forming ternary

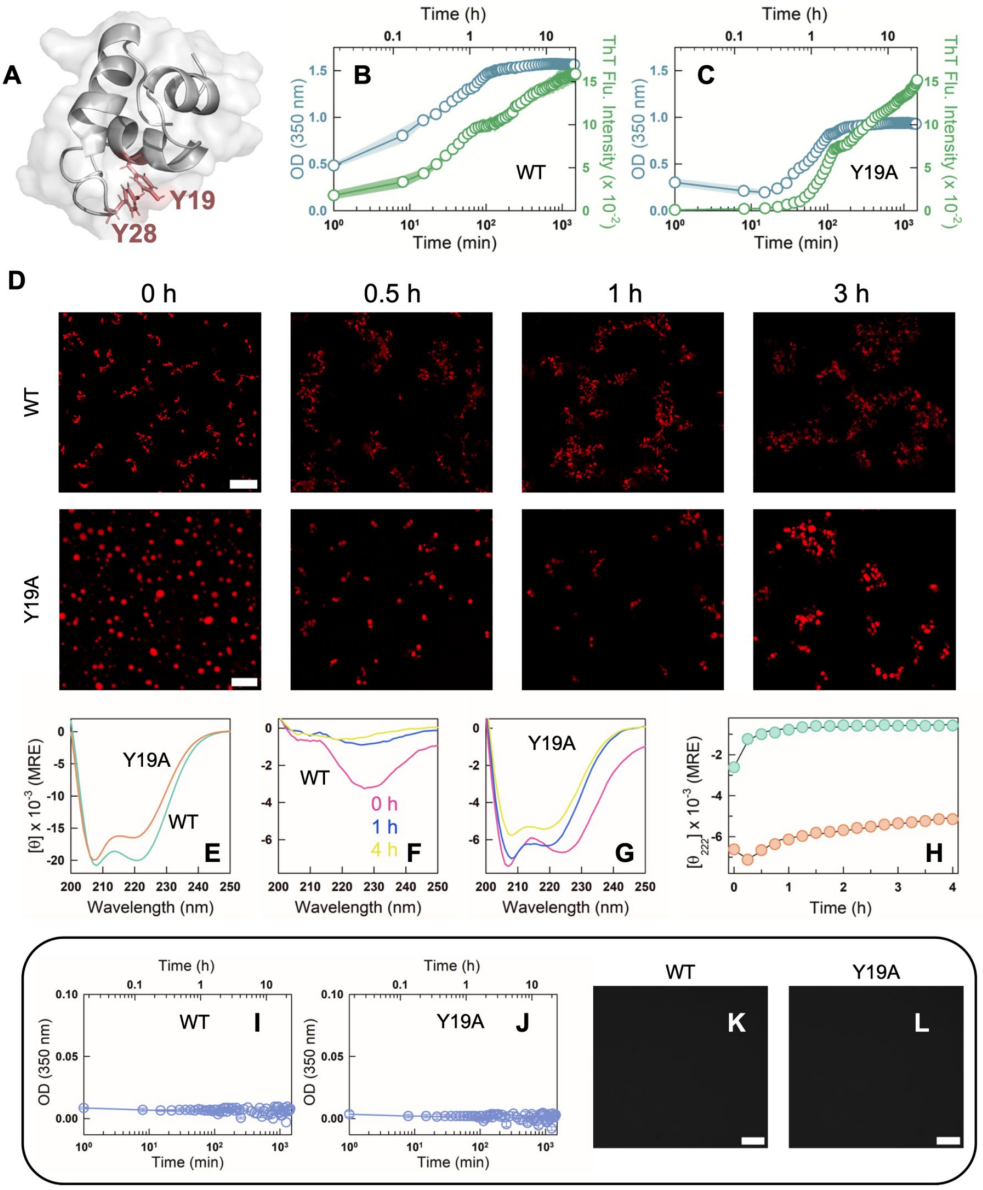

Figure 6

PolyP is able to discriminate between folded and molten-globular variants of FruR DBD while DNA does not.

(A) 3D structure of the DNA binding domain of FruR highlighting an aromatic stacking interaction between Y19 and Y28. (B, C) Turbidity (blue circles and left y-axis) and ThT fluorescence intensity (green circles and right y-axis) curve for 90 μM FruR WT (B) and Y19A (C) in the presence of 22 μM polyP. The mean data from N= 2 experiments and the corresponding spread are shown as circles and shaded area, respectively. (D) Representative fluorescence microscopy images of NHS-rhodamine labeled FruR WT (top panel) and Y19A (bottom panel) in the presence of polyP at different time points (0, 0.5,1 and 3 hours). The scale bar is 10 μm. (E) Far-UV CD spectra of FruR WT (green) and Y19A (red) at 298 K in mean residue ellipticity (MRE) units of deg. cm^2 $dmol^{-1}$ in the absence of polyP. (F and G) Far-UV CD spectra of 55 μM FruR WT (F) and Y19A (G) at different time points - 0 hour (pink), 1 hour (blue), and 4 hours (yellow) - after the addition of 22 μM polyP at 298 K and displayed in mean residue ellipticity (MRE). Note that the y-axis scales of this panel is different from panel E. (H) Time dependence of the signal at 222 nm for WT (green) and Y19A (red). (I and J) Turbidity of 25 μM WT (I) and Y19A (J) with 1 μM DNA as a function of time from N = 2 experiments. No changes in turbidity are observed with time. (K and L) Representative fluorescence microscopy images of NHS-rhodamine labeled FruR WT (K) and Y19A (L) in the presence of DNA. The scale bar is 10 μm.

condensates regulating gene expression, as shown in studies on the bacterial protein Hfq.[27] Taken together with our results on CytR, caution needs to be exercised in interpreting in-cell microscopy results, as it is possible that polyP is involved in condensates, especially when proteins of interest are rich in basic residues. Finally, the full length CytR plays an important role in transcription regulation of genes involved in stress response, including critical roles in nucleoside catabolism, context-dependent activation or repression, and pathogenesis.[59–61] CytR also binds to the promotor region of the rpoH gene and represses transcription, thus regulating the expression of σ^{32} – an RNA polymerase subunit essential for the transcription of heat shock proteins.[62,63] Given the results of the current work and since polyP concentrations rise significantly in stressed cells,[20] it is tempting to speculate that polyP interacts with CytR to form condensates and sequesters it, thus promoting σ^{32} transcription. Studies on CytR combining other stress response regulators, specifically with the nucleoid-associated sensory protein H-NS, with DNA and polyP could unravel hitherto unexplored mechanisms regulating the nuanced gene expression patterns in enterobacteria.

Supplementary figures

Figure S1

Fluorescence microscopy images of 90 μM WT with 22 μM polyP at 160 mM ionic strength (pH 7) immediately after adding polyP (left panel) and after 30 minutes (right panel).

The scale bar is 10 μm.

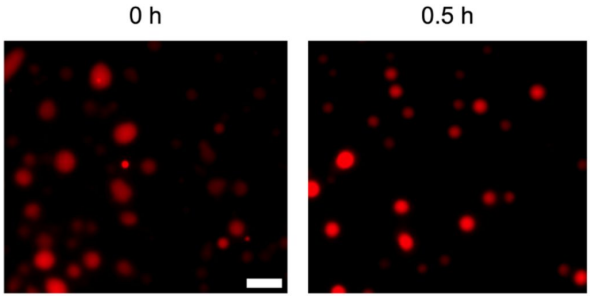

Figure S2

Turbidity (blue circles and left y-axis) and ThT fluorescence intensity (green circles and right y-axis) curve for 90 μM WT (left panel), DM (middle panel), and P33A (right panel) in the presence of 5 μM ThT.

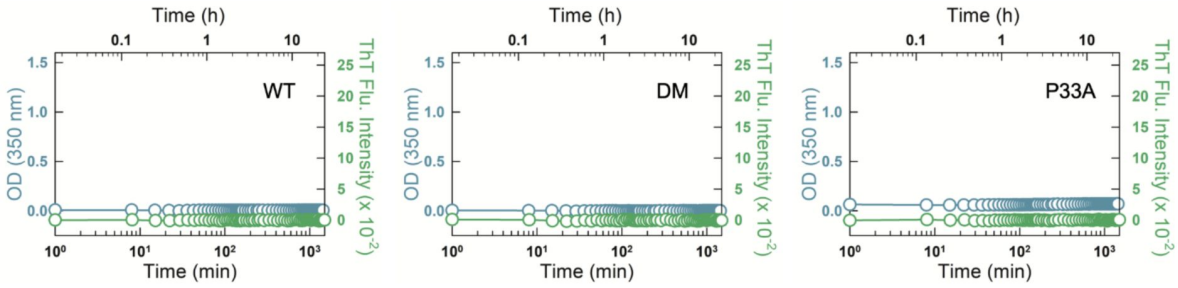

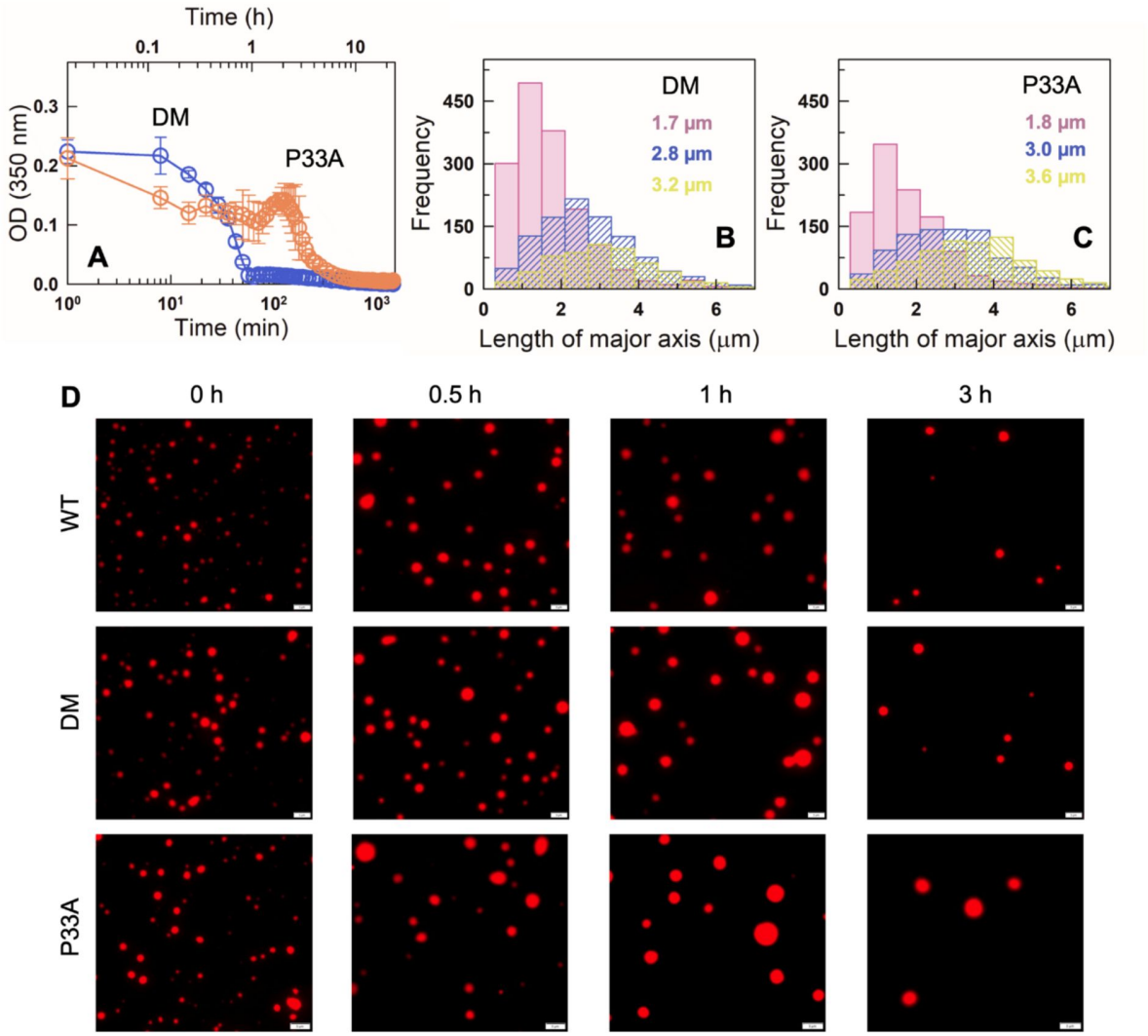

Figure S3

(A) Turbidity of 25 μM DM (blue) and P33A (orange) with 1 μM DNA as a function of time. The mean and the spread from N = 2experiments are shown as circles and error bar, respectively. (B, C) Droplet size-distributions for DM (B) and P33A (C) in the presence of DNA at different time points: 0 min (pink), 30 min (blue), and 60 min (yellow). Values given in the plot represent the mean dimensions of droplets at the corresponding time points. (D) Fluorescence microscopy images of NHS-rhodamine labeled WT (top), DM (middle) and P33A (bottom) in the presence of 45 bp DNA at different time points. The scale bar is 5 μm.

Figure S4

FRAP experiments for CytR variants in the presence of DNA at different time points: 0 min (pink), 30 min (blue), and 60 min (yellow).

Data are reported as mean ± s.d. for N = 4 experiments. (A-C) FRAP recovery curves of NHS-rhodamine labeled WT (A), DM (B) and P33A (C). The experimental errors are smaller than the size of data points. (D, F, H) FRAP recovery half-times for WT (D), DM (F), and P33A (H) at the indicated time points. (E, G, H) Recovery amplitude plots for WT (E), DM (G) and P33A (I) at different time points.

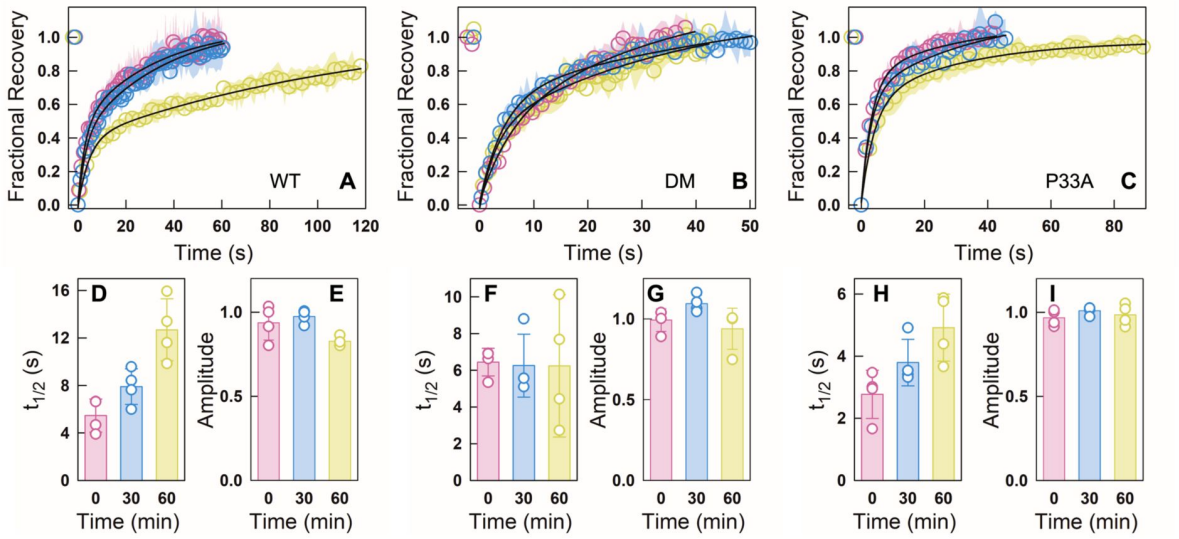

Figure S5

Fluorescence microscopy images of 90 μM NHS-rhodamine labeled WT (top), DM (middle) and P33A (bottom) in the presence of 11.24 μM of 45-bp DNA at the time points indicated.

The scale bar is 10 μm.

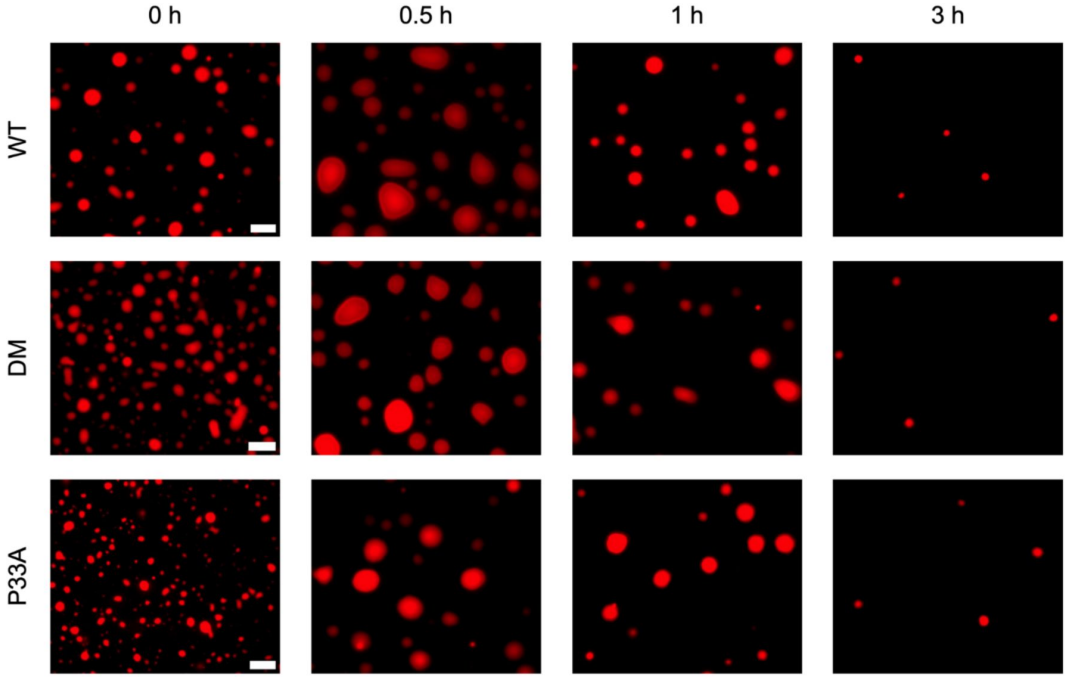

Figure S6

FTIR spectra of WT (left), DM (middle), and P33A (right) showing normalized absorbance recorded at a wavenumber range of 1700 – 1600 cm^{-1}.

Black curves represent FTIR spectra of protein in the absence of DNA, and blue and green curves show FTIR spectra of protein after the addition of DNA at 0 min and 60 min, respectively.

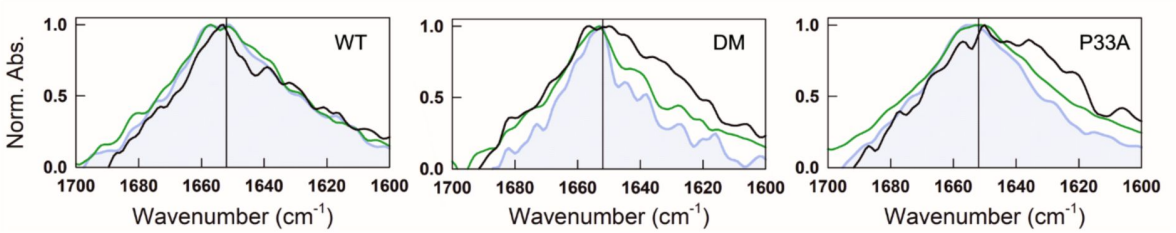

Figure S7

FRAP experiments on Y19A variant of FruR in the presence of polyP at different time points: 0 - 10 min (pink), 10-20 min (blue), and 20-30 min (yellow).

(A) FRAP recovery curves of NHS-rhodamine labeled FruR. Arrow indicates the movement of the recovery profiles at longer incubation times. (B) Recovery half-time at the indicated time points. (C) Recovery amplitude at different time points. FRAP data for 0-10 min represents data from a single experiment as the condensates of Y19A are highly metastable (also see **Figure 6C**). The data acquired between 10-20 and 20-30 minutes are shown as mean ± s.d from N = 4 and 3 experiments, respectively. The experimental errors are smaller than the size of data points.

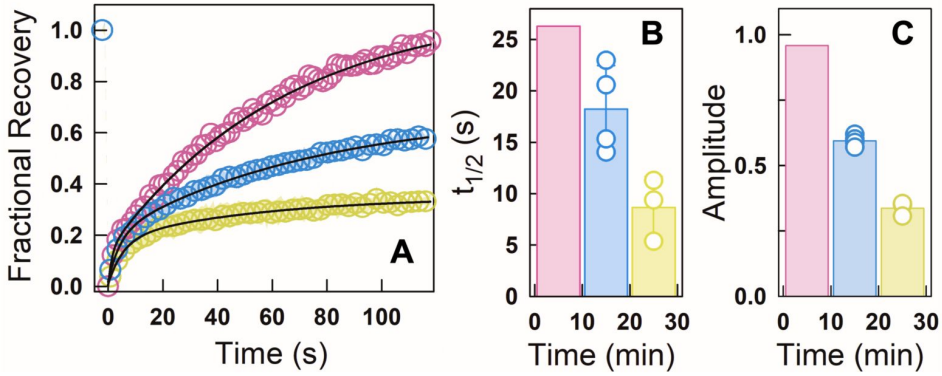

Acknowledgements

The authors are grateful for the support from the Department of Biotechnology (DBT, India) for the grant BT/PR41973/BRB/10/1967/2021 to A. N. N. The authors acknowledge the FIST facility (SR/FST/LS-II/2020/552(C)) sponsored by the Department of Science and Technology (DST, India) and the ICSR - Common Instruments Facility (CIF) at the Department of Biotechnology, IIT Madras (Chennai, India) for the instrumentation. The authors thank Vijay Rangachari and Ethayaraja Mani for the discussions, Swathi Sudhakar for the help in flow chamber preparation, and Thalappil Pradeep and Sonali Seth for help in FTIR experiments. D.R. acknowledges Women Leading IITM for the funding.

Additional information

Abbreviations

- polyP: polyphosphate
- CytR: cytidine repressor
- LLPS: liquid-liquid phase separation
- DIC: differential interference contrast
- CD: circular dichroism
- FTIR: Fourier-transform infra-red
- DNA: deoxy ribonucleic acid

References

(1) Brangwynne C. P., Eckmann C. R., Courson D. S., Rybarska A., Hoege C., Gharakhani J., Jülicher F., Hyman A. A (2009) **Germline P Granules Are Liquid Droplets That Localize by Controlled Dissolution/Condensation** *Science (1979)* **324**:1729–1732 https://doi.org/10.1126/science.1172046 | Google Scholar

(2) Hyman A. A., Brangwynne C. P (2011) **Beyond Stereospecificity: Liquids and Mesoscale Organization of Cytoplasm** *Dev. Cell* **21**:14–16 https://doi.org/10.1016/j.devcel.2011.06.013 | Google Scholar

(3) Shin Y., Brangwynne C. P (2017) **Liquid Phase Condensation in Cell Physiology and Disease** *Science (1979)* **357** https://doi.org/10.1126/science.aaf4382 | Google Scholar

(4) Banani S. F., Lee H. O., Hyman A. A., Rosen M. K (2017) **Biomolecular Condensates: Organizers of Cellular Biochemistry** *Nat. Rev. Mol. Cell Biol* **18**:285–298 https://doi.org/10.1038/nrm.2017.7 | Google Scholar

(5) Alberti S., Hyman A. A (2021) **Biomolecular Condensates at the Nexus of Cellular Stress, Protein Aggregation Disease and Ageing** *Nat. Rev. Mol. Cell Biol* **22**:196–213 https://doi.org/10.1038/s41580-020-00326-6 | Google Scholar

(6) Shapiro D. M., Ney M., Eghtesadi S. A., Chilkoti A (2021) **Protein Phase Separation Arising from Intrinsic Disorder: First-Principles to Bespoke Applications** *J. Phys. Chem. B* **125**:6740–6759 https://doi.org/10.1021/acs.jpcb.1c01146 | Google Scholar

(7) Pappu R. V, Cohen S. R., Dar F., Farag M., Kar M (2023) **Phase Transitions of Associative Biomacromolecules** *Chem. Rev* **123**:8945–8987 https://doi.org/10.1021/acs.chemrev.2c00814 | Google Scholar

(8) Zhou H.-X., Kota D., Qin S., Prasad R (2024) **Fundamental Aspects of Phase-Separated Biomolecular Condensates** *Chem. Rev* **124**:8550–8595 https://doi.org/10.1021/acs.chemrev.4c00138 | Google Scholar

(9) Rai S. K., Savastano A., Singh P., Mukhopadhyay S., Zweckstetter M (2021) **Liquid-Liquid Phase Separation of Tau: From Molecular Biophysics to Physiology and Disease** *Prot. Sci* **30**:1294–1314 https://doi.org/10.1002/pro.4093 | Google Scholar

(10) Agarwal A., Mukhopadhyay S (2022) **Prion Protein Biology Through the Lens of Liquid-Liquid Phase Separation** *J. Mol. Biol* **434**:167368 https://doi.org/10.1016/j.jmb.2021.167368 | Google Scholar

(11) Rangachari V (2023) **Biomolecular Condensates - Extant Relics or Evolving Microcompartments?** *Commun. Biol.* **6**:656 https://doi.org/10.1038/s42003-023-04963-3 | Google Scholar

(12) Mukherjee S., Poudyal M., Dave K., Kadu P., Maji S. K (2024) **Protein Misfolding and Amyloid Nucleation through Liquid-Liquid Phase Separation** *Chem. Soc. Rev* **53**:4976–5013 https://doi.org/10.1039/d3cs01065a | Google Scholar

(13) Larson A. G., Elnatan D., Keenen M. M., Trnka M. J., Johnston J. B., Burlingame A. L., Agard D. A., Redding S., Narlikar G. J (2017) **Liquid Droplet Formation by HP1α Suggests a Role for Phase Separation in Heterochromatin** *Nature* **547**:236–240 https://doi.org/10.1038/nature22822 | Google Scholar

(14) Strom A. R., Emelyanov A. V, Mir M., Fyodorov D. V, Darzacq X., Karpen G. H (2017) **Phase Separation Drives Heterochromatin Domain Formation** *Nature* **547**:241–245 https://doi.org/10.1038/nature22989 | Google Scholar

(15) Vieregg J. R., Lueckheide M., Marciel A. B., Leon L., Bologna A. J., Rivera J. R., Tirrell M. V (2018) **Oligonucleotide-Peptide Complexes: Phase Control by Hybridization** *J. Am. Chem. Soc* **140**:1632–1638 https://doi.org/10.1021/jacs.7b03567 | Google Scholar

(16) Dutagaci B., Nawrocki G., Goodluck J., Ashkarran A. A., Hoogstraten C. G., Lapidus L. J., Feig M (2021) **Charge-Driven Condensation of RNA and Proteins Suggests Broad Role of Phase Separation in Cytoplasmic Environments** *eLife* **10** https://doi.org/10.7554/eLife.64004 | Google Scholar

(17) King J. T., Shakya A (2021) **Phase Separation of DNA: From Past to Present** *Biophys. J* **120**:1139–1149 https://doi.org/10.1016/j.bpj.2021.01.033 | Google Scholar

(18) Phan T. M., Kim Y. C., Debelouchina G. T., Mittal J (2024) **Interplay between Charge Distribution and DNA in Shaping HP1 Paralog Phase Separation and Localization** *eLife* **12** https://doi.org/10.7554/eLife.90820 | Google Scholar

(19) Nordenskiöld L., Shi X., Korolev N., Zhao L., Zhai Z., Lindman B (2024) **Liquid-Liquid Phase Separation (LLPS) in DNA and Chromatin Systems from the Perspective of Colloid Physical Chemistry** *Adv. Coll. Int. Sci* **326** https://doi.org/10.1016/j.cis.2024.103133 | Google Scholar

(20) Kornberg A., Rao N. N., Ault-Riché D (1999) **Inorganic Polyphosphate: A Molecule of Many Functions** *Ann. Rev. Biochem* **68**:89–125 https://doi.org/10.1146/annurev.biochem.68.1.89 | Google Scholar

(21) Brown M. R. W., Kornberg A (2004) **Inorganic Polyphosphate in the Origin and Survival of Species** *Proc. Natl. Acad. Sci. U. S. A* **101**:16085–16087 https://doi.org/10.1073/pnas.0406909101 | Google Scholar

(22) Rao N. N., Gómez-García M. R., Kornberg A (2009) **Inorganic Polyphosphate: Essential for Growth and Survival** *Ann. Rev. Biochem* **78**:605–647 https://doi.org/10.1146/annurev.biochem.77.083007.093039 | Google Scholar

(23) Shi X., Rao N. N., Kornberg A (2004) **Inorganic Polyphosphate in Bacillus Cereus: Motility, Biofilm Formation, and Sporulation** *Proc. Natl. Acad. Sci. U. S. A* **101**:17061–17065 https://doi.org/10.1073/pnas.0407787101 | Google Scholar

(24) Xie L., Rajpurkar A., Quarles E., Taube N., Rai A. S., Erba J., Sliwinski B., Markowitz M., Jakob U., Knoefler D (2019) **Accumulation of Nucleolar Inorganic Polyphosphate Is a Cellular**

Response to Cisplatin-Induced Apoptosis *Front. Oncol.* **9**:1410 https://doi.org/10.3389/fonc.2019.01410 | Google Scholar

(25) Müller W. E. G., Schröder H. C., Wang X (2019) **Inorganic Polyphosphates As Storage for and Generator of Metabolic Energy in the Extracellular Matrix** *Chem. Rev* **119**:12337–12374 https://doi.org/10.1021/acs.chemrev.9b00460 | Google Scholar

(26) Beaufay F., Quarles E., Franz A., Katamanin O., Wholey W.-Y., Jakob U (2020) **Polyphosphate Functions In Vivo as an Iron Chelator and Fenton Reaction Inhibitor** *mBio* **11** https://doi.org/10.1128/mBio.01017-20 | Google Scholar

(27) Beaufay F., Amemiya H. M., Guan J., Basalla J., Meinen B. A., Chen Z., Mitra R., Bardwell J. C. A., Biteen J. S., Vecchiarelli A. G., Freddolino P. L., Jakob U (2021) **Polyphosphate Drives Bacterial Heterochromatin Formation** *Sci. Adv* **7**:eabk0233 https://doi.org/10.1126/sciadv.abk0233 | Google Scholar

(28) Solesio M. E., Xie L., McIntyre B., Ellenberger M., Mitaishvili E., Bhadra-Lobo S., Bettcher L. F., Bazil J. N., Raftery D., Jakob U., Pavlov E. V (2021) **Depletion of Mitochondrial Inorganic Polyphosphate (PolyP) in Mammalian Cells Causes Metabolic Shift from Oxidative Phosphorylation to Glycolysis** *Biochem. J* **478**:1631–1646 https://doi.org/10.1042/BCJ20200975 | Google Scholar

(29) Gray M. J., Wholey W.-Y., Wagner N. O., Cremers C. M., Mueller-Schickert A., Hock N. T., Krieger A. G., Smith E. M., Bender R. A., Bardwell J. C. A., Jakob U (2014) **Polyphosphate Is a Primordial Chaperone** *Mol. Cell* **53**:689–699 https://doi.org/10.1016/j.molcel.2014.01.012 | Google Scholar

(30) Cremers C. M., Knoefler D., Gates S., Martin N., Dahl J.-U., Lempart J., Xie L., Chapman M. R., Galvan V., Southworth D. R., Jakob U (2016) **Polyphosphate: A Conserved Modifier of Amyloidogenic Processes** *Mol. Cell* **63**:768–780 https://doi.org/10.1016/j.molcel.2016.07.016 | Google Scholar

(31) Yoo N. G., Dogra S., Meinen B. A., Tse E., Haefliger J., Southworth D. R., Gray M. J., Dahl J.-U., Jakob U (2018) **Polyphosphate Stabilizes Protein Unfolding Intermediates as Soluble Amyloid-like Oligomers** *J. Mol. Biol* **430**:4195–4208 https://doi.org/10.1016/j.jmb.2018.08.016 | Google Scholar

(32) Xie L., Jakob U (2019) **Inorganic Polyphosphate, a Multifunctional Polyanionic Protein Scaffold** *J. Biol. Chem* **294**:2180–2190 https://doi.org/10.1074/jbc.REV118.002808 | Google Scholar

(33) Guan J., Jakob U (2024) **The Protein Scaffolding Functions of Polyphosphate** *J. Mol. Biol* **436**:168504 https://doi.org/10.1016/j.jmb.2024.168504 | Google Scholar

(34) Erdős G., Pajkos M., Dosztányi Z (2021) **IUPred3: Prediction of Protein Disorder Enhanced with Unambiguous Experimental Annotation and Visualization of Evolutionary Conservation** *Nuc. Acids Res* **49**:W297–W303 https://doi.org/10.1093/nar/gkab408 | Google Scholar

(35) Jurrus E., Engel D., Star K., Monson K., Brandi J., Felberg L. E., Brookes D. H., Wilson L., Chen J., Liles K., Chun M., Li P., Gohara D. W., Dolinsky T., Konecny R., Koes D. R., Nielsen J. E., Head-Gordon T., Geng W., Krasny R., Wei G. W., Holst M. J., McCammon J. A., Baker N. A (2018)

Improvements to the APBS Biomolecular Solvation Software Suite *Protein Sci* **27**:112–128 https://doi.org/10.1002/pro.3280 | Google Scholar

(36) Moody C. L., Tretyachenko-Ladokhina V., Laue T. M., Senear D. F., Cocco M. J (2011) **Multiple Conformations of the Cytidine Repressor DNA-Binding Domain Coalesce to One upon Recognition of a Specific DNA Surface** *Biochemistry* **50**:6622–6632 https://doi.org/10.1021/bi200205v | Google Scholar

(37) Munshi S., Rajendran D., Naganathan A. N (2018) **Entropic Control of an Excited Folded-Like Conformation in a Disordered Protein Ensemble** *J. Mol. Biol* **430**:2688–2694 https://doi.org/10.1016/j.jmb.2018.06.008 | Google Scholar

(38) Munshi S., Subramanian S., Ramesh S., Golla H., Kalivarathan D., Kulkarni M., Campos L. A., Sekhar A., Naganathan A. N (2019) **Engineering Order and Cooperativity in a Disordered Protein** *Biochemistry* **58**:2389–2397 https://doi.org/10.1021/acs.biochem.9b00182 | Google Scholar

(39) Munshi S., Rajendran D., Ramesh S., Subramanian S., Bhattacharjee K., Kumar M. R., Naganathan A. N (2020) **Controlling Structure and Dimensions of a Disordered Protein via Mutations** *Biochemistry* **59**:171–174 https://doi.org/10.1021/acs.biochem.9b00678 | Google Scholar

(40) Madhurima K., Nandi B., Munshi S., Naganathan A. N., Sekhar A (2023) **Functional Regulation of an Intrinsically Disordered Protein via a Conformationally Excited State** *Sci. Adv* **9**:eadh4591 https://doi.org/10.1126/sciadv.adh4591 | Google Scholar

(41) Munshi S., Gopi S., Subramanian S., Campos L. A., Naganathan A. N (2018) **Protein Plasticity Driven by Disorder and Collapse Governs the Heterogeneous Binding of CytR to DNA** *Nucleic Acids Res* **46**:4044–4053 Google Scholar

(42) Munshi S., Gopi S., Asampille G., Subramanian S., Campos L. A., Atreya H. S., Naganathan A. N (2018) **Tunable Order-Disorder Continuum in Protein-DNA Interactions** *Nucleic Acids Res* **46**:8700–8709 https://doi.org/10.1093/nar/gky732 | Google Scholar

(43) Sudhakar S., Abdosamadi M. K., Jachowski T. J., Bugiel M., Jannasch A., Schäffer E (2021) **Germanium Nanospheres for Ultraresolution Picotensiometry of Kinesin Motors** *Science (1979)* **371** https://doi.org/10.1126/science.abd9944 | Google Scholar

(44) Schneider C. A., Rasband W. S., Eliceiri K. W (2012) **NIH Image to ImageJ: 25 Years of Image Analysis** *Nat. Methods* **9**:671–675 https://doi.org/10.1038/nmeth.2089 | Google Scholar

(45) Poudyal M., Patel K., Gadhe L., Sawner A. S., Kadu P., Datta D., Mukherjee S., Ray S., Navalkar A., Maiti S., Chatterjee D., Devi J., Bera R., Gahlot N., Joseph J., Padinhateeri R., Maji S. K (2023) **Intermolecular Interactions Underlie Protein/Peptide Phase Separation Irrespective of Sequence and Structure at Crowded Milieu** *Nat. Commun* **14**:6199 https://doi.org/10.1038/s41467-023-41864-9 | Google Scholar

(46) Patel A., Lee H. O., Jawerth L., Maharana S., Jahnel M., Hein M. Y., Stoynov S., Mahamid J., Saha S., Franzmann T. M., Pozniakovski A., Poser I., Maghelli N., Royer L. A., Weigert M., Myers E. W., Grill S., Drechsel D., Hyman A. A., Alberti S (2015) **A Liquid-to-Solid Phase Transition of the ALS Protein FUS Accelerated by Disease Mutation** *Cell* **162**:1066–1077 https://doi.org/10.1016/j.cell.2015.07.047 | Google Scholar

(47) Ray S., Singh N., Kumar R., Patel K., Pandey S., Datta D., Mahato J., Panigrahi R., Navalkar A., Mehra S., Gadhe L., Chatterjee D., Sawner A. S., Maiti S., Bhatia S., Gerez J. A., Chowdhury A., Kumar A., Padinhateeri R., Riek R., Krishnamoorthy G., Maji S. K (2020) **α-Synuclein Aggregation Nucleates through Liquid-Liquid Phase Separation** *Nat. Chem* **12**:705–716 https://doi.org/10.1038/s41557-020-0465-9 | Google Scholar

(48) Shen Y., Chen A., Wang W., Shen Y., Ruggeri F. S., Aime S., Wang Z., Qamar S., Espinosa J. R., Garaizar A., St George-Hyslop P., Collepardo-Guevara R., Weitz D. A., Vigolo D., Knowles T. P. J (2023) **The Liquid-to-Solid Transition of FUS Is Promoted by the Condensate Surface** *Proc. Natl. Acad. Sci. U. S. A. atl* **120**:e2301366120 https://doi.org/10.1073/pnas.2301366120 | Google Scholar

(49) Gracia P., Polanco D., Tarancón-Díez J., Serra I., Bracci M., Oroz J., Laurents D. V, García I., Cremades N (2022) **Molecular Mechanism for the Synchronized Electrostatic Coacervation and Co-Aggregation of Alpha-Synuclein and Tau** *Nat. Comm* **13**:4586 https://doi.org/10.1038/s41467-022-32350-9 | Google Scholar

(50) Dhakal S., Mondal M., Mirzazadeh A., Banerjee S., Ghosh A., Rangachari V (2023) **α-Synuclein Emulsifies TDP-43 Prion-like Domain-RNA Liquid Droplets to Promote Heterotypic Amyloid Fibrils** *Comm. Biol.* **6**:1227 https://doi.org/10.1038/s42003-023-05608-1 | Google Scholar

(51) Shi Z., Woody R. W., Kallenbach N. R (2002) **Is Polyproline II a Major Backbone Conformation in Unfolded Proteins?** *Adv. Protein Chem* **62**:163–240 Google Scholar

(52) Kelly S. M., Price N. C (2000) **The Use of Circular Dichroism in the Investigation of Protein Structure and Function** *Curr. Prot. Pept. Sci* **1**:349–384 https://doi.org/10.2174/1389203003381315 | Google Scholar

(53) Rajendran D., Goyal S., Chaurasiya D. K., Naganathan A. N (2024) **Determinants of Unfolding Cooperativity and Binding Are Decoupled in a DNA Binding Domain** *J. Phys. Chem. B* **128**:9341–9352 https://doi.org/10.1021/acs.jpcb.4c03895 | Google Scholar

(54) Murthy A. C., Dignon G. L., Kan Y., Zerze G. H., Parekh S. H., Mittal J., Fawzi N. L (2019) **Molecular Interactions Underlying Liquid-Liquid Phase Separation of the FUS Low-Complexity Domain** *Nat. Struct. Mol. Biol* **26**:637–648 https://doi.org/10.1038/s41594-019-0250-x | Google Scholar

(55) Wen J., Hong L., Krainer G., Yao Q.-Q., Knowles T. P. J., Wu S., Perrett S (2021) **Conformational Expansion of Tau in Condensates Promotes Irreversible Aggregation** *J. Am. Chem. Soc* **143**:13056–13064 https://doi.org/10.1021/jacs.1c03078 | Google Scholar

(56) Ubbiali D., Fratini M., Piersimoni L., Ihling C. H., Kipping M., Heilmann I., Iacobucci C., Sinz A (2022) **Direct Observation of "Elongated" Conformational States in α-Synuclein upon Liquid-Liquid Phase Separation** *Ang. Chemie* **61**:e202205726 https://doi.org/10.1002/anie.202205726 | Google Scholar

(57) Joshi A., Walimbe A., Avni A., Rai S. K., Arora L., Sarkar S., Mukhopadhyay S (2023) **Single-Molecule FRET Unmasks Structural Subpopulations and Crucial Molecular Events during FUS Low-Complexity Domain Phase Separation** *Nat. Comm* **14**:7331 https://doi.org/10.1038/s41467-023-43225-y | Google Scholar

(58) Wang X., Shi C., Mo J., Xu Y., Wei W., Zhao J (2020) **An Inorganic Biopolymer Polyphosphate Controls Positively Charged Protein Phase Transitions** *Ang. Chemie* **59**:2679–2683 https://

doi.org/10.1002/anie.201913833 | Google Scholar

(59) Barbier C. S., Short S. A (1992) **Amino-acid substitutions in the cytr repressor which alter its capacity to regulate gene-expression** *J. Bacteriol* **174**:2881–2890 Google Scholar

(60) Rasmussen P. B., Holst B., Valentin-Hansen P (1996) **Dual-Function Regulators: The CAMP Receptor Protein and the CytR Regulator Can Act Either to Repress or to Activate Transcription Depending on the Context** *Proc. Natl. Acad. Sci. U. S. A* **93**:10151–10155 https://doi.org/10.1073/pnas.93.19.10151 | Google Scholar

(61) Hirakawa H., Takita A., Kato M., Mizumoto H., Tomita H (2020) **Roles of CytR, an Anti-Activator of Cyclic-AMP Receptor Protein (CRP) on Flagellar Expression and Virulence in Uropathogenic Escherichia Coli** *Biochem. Biophys. Res. Commun* **521**:555–561 https://doi.org/10.1016/j.bbrc.2019.10.165 | Google Scholar

(62) Kallipolitis B. H., Valentin-Hansen P. (1998) **Transcription of RpoH, Encoding the Escherichia Coli Heat-Shock Regulator Sigma32, Is Negatively Controlled by the CAMP-CRP/CytR Nucleoprotein Complex** *Mol. Microbiol* **29**:1091–1099 https://doi.org/10.1046/j.1365-2958.1998.00999.x | Google Scholar

(63) Lauritsen I., Frendorf P. O., Capucci S., Heyde S. A. H., Blomquist S. D., Wendel S., Fischer E. C., Sekowska A., Danchin A., Nørholm M. H. H (2021) **Temporal Evolution of Master Regulator Crp Identifies Pyrimidines as Catabolite Modulator Factors** *Nat. Commun* **12**:5880 https://doi.org/10.1038/s41467-021-26098-x | Google Scholar

Author information

Saloni Goyal
Department of Biotechnology, Bhupat & Jyoti Mehta School of Biosciences, Indian Institute of Technology Madras, Chennai, India

Divya Rajendran
Department of Biotechnology, Bhupat & Jyoti Mehta School of Biosciences, Indian Institute of Technology Madras, Chennai, India

Anup Kumar Mani
Department of Biotechnology, Bhupat & Jyoti Mehta School of Biosciences, Indian Institute of Technology Madras, Chennai, India

Athi N Naganathan
Department of Biotechnology, Bhupat & Jyoti Mehta School of Biosciences, Indian Institute of Technology Madras, Chennai, India
ORCID iD: 0000-0002-1655-7802

For correspondence: athi@iitm.ac.in

Editors

Reviewing Editor
Julien Roche
Iowa State University, Ames, United States of America

Senior Editor
Qiang Cui
Boston University, Boston, United States of America

Reviewer #1 (Public review):

In the article Goyal and colleagues investigate the role of negatively charged biopolymers, i.e., polyphosphate (polyP) and DNA, play in phase separation of cytidine repressor (CytR) and fructose repressor (FruR). The authors find that both negative polymers drive the formation of metastable protein/polymer condensates. However, polyP-driven condensates form more gel- or solid-like structures over time while DNA-driven condensates tend to dissipate over time. The authors link this disparate condensate behavior to polyP-induced structures within the enzymes. Specifically, they observe the formation of polyproline II-like structures within two tested enzyme variants in the presence of polyP. Together, their results provide a unique insight into the physical and structural mechanism by which two unique negatively charged polymers can induce distinct phase transitions with the same protein. This study will be a welcomed addition to the condensate field and provide new molecular insights into how binding partner-induced structural changes within a given protein can affect the mesoscale behavior of condensates.

https://doi.org/10.7554/eLife.105461.2.sa2

Reviewer #2 (Public review):

Summary:

In the article Goyal et al. investigate how protein/polymer phase transition behavior is modulated by different binding partners-specifically, DNA and polyphosphate (PolyP). The authors show that while both DNA and PolyP can induce metastable condensates, only PolyP drives unique phase transition behaviors by effectively discriminating among initial protein ensembles with varying degrees of conformational heterogeneity, compactness, and plasticity. This selectivity is attributed to PolyP's ability to unfold the enzyme during condensate formation, supported by the observation of polyproline II-rich structures in two tested variants (CytR WT and DM). Overall, this work offers valuable insights into the mechanistic factors underlying condensation assembly and advances our understanding of how molecular interactions influence phase behavior.

Strengths:

The authors employed a well-designed and technically sound experimental approach to investigate how the initial protein conformational ensemble influences phase transition behavior in the presence of two charged polymers. Specifically, they examined phase transitions of CytR and FruR variants in the context of either polyphosphate (PolyP) or DNA, enabling a direct comparison that effectively highlights key differences. This study provides mechanistic insights into the role of PolyP in driving condensation and may contribute to a broader understanding of assembly processes involving PolyP, particularly in the context of bacterial stress responses.

Weaknesses:

The primary weakness of this manuscript lies in the lack of a consistent trend linking the unique phase transitions observed in protein/PolyP systems to the initial protein conformational ensemble. The observed differences in assembly and maturation behavior do not consistently correlate with conformational heterogeneity, plasticity, or compactness of the starting ensemble. This is particularly evident in the divergent outcomes between the CytR/PolyP and FruR/PolyP systems. Consequently, the phase behavior of protein/PolyP condensates does not reliably reflect the composition of the initial conformational ensemble, limiting its effectiveness as a probe for conformational state characterization.

https://doi.org/10.7554/eLife.105461.2.sa1

Author response:

The following is the authors' response to the original reviews.

> ***Reviewer 1:***
>
> *In the article titled "Polyphosphate discriminates protein conformational ensembles more efficiently than DNA promoting diverse assembly and maturation behaviors," Goyal and colleagues investigate the role of negatively charged biopolymers, i.e., polyphosphate (polyP) and DNA, play in phase separation of cytidine repressor (CytR) and fructose repressor (FruR). The authors find that both negative polymers drive the formation of metastable protein/polymer condensates. However, polyPdriven condensates form more gel- or solid-like structures over time while DNA-driven condensates tend to dissipate over time. The authors link this disparate condensate behavior to polyP-induced structures within the enzymes. Specifically, they observe the formation of polyproline II-like structures within two tested enzyme variants in the presence of polyP. Together their results provide a unique insight into the physical and structural mechanism by which two unique negatively charged polymers can induce distinct phase transitions with the same protein. This study will be a welcomed addition to the condensate field and provide new molecular insights into how binding partner-induced structural changes within a given protein can affect the mesoscale behavior of condensates. The concerns outlined below are meant to strengthen the manuscript.*
>
> *Recommendation:*

We value the reviewer's positive comments and appreciate time taken to provide detailed feedback that has certainly helped improve our manuscript.

> *Major Concerns:*
>
> *(1) The biggest concern in this manuscript lies with experiments comparing polyP45, which has a net negative charge of -47, and double-stranded DNA of 45 base pairs (as stated in the methods), which will have a net negative charge of -90. Given the dependence of phase separation and phase transitions on not only net charge but charge density, this is an important factor to consider when comparing the effect of these molecules. It is unclear how or if the authors considered these factors in the design of their experiments. Because of the factor of 2 difference in net charge over the same number of polymer chain components, i.e. a chain of 45 pi vs. a chain of 45 double-stranded base pairs, it is unclear if the results from polyP vs. DNA are directly comparable. One solution would be to repeat all DNA experiments using single-stranded DNA so that the net charge is similar to polyP over the same chain length. Another*

> *possibility would be to repeat DNA experiments using a doublestranded DNA of 23 base pairs. This would allow for a nearly equal net charge (-46 vs. -47 for polyP), but the charge density would still be 2X polyP. As it stands now, the perceived differences in DNA vs. polyP behavior may be an artifact arising from the difference in net charge and charge density between DNA and polyP.*

To address the reviewer's concerns regarding charge density differences between polyP and DNA, we conducted an experiment using a higher DNA concentration (11.24 μM) to obtain charge equivalence between the two experiments (i.e. the total concentration of charges). As shown in Figure S5, even at higher DNA concentration, the condensates undergo progressive dissolution over time. This observation indicates that the differential maturation of condensates, arising from distinct initial protein ensembles, are governed by the intrinsic properties of polyP. Charge density (i.e. the number of charges per unit volume of the polymer), on the other hand, is an intrinsic feature of the polymer which is naturally different between DNA and polyP. In fact, the primary result of our work is our observation that polyP can discern the starting ensembles more efficiently, likely through actively engaging and interacting with the ensemble while DNA appears to be a passive player. The differences are not an artifact as they arise from fundamental features of two natural anionic polymers found within cells. In other words, the outcomes could be very different if the concentration of one polymer dominates over the other (see the response below).

> *(2) One outstanding question the authors do not address relates to how mixtures of CytR or FruR, DNA, and polyP behave. In the bacterial cytoplasm, these molecules are all in the same compartment (admittedly that compartment is not well mixed due to unique condensate-driven organization). Would the authors expect to see similar effects of polyP and DNA if they were in the same solution? Perhaps the authors could run a set of experiments where they vary the ratios of DNA and polyP to probe how increased levels of "stress", i.e. increased levels of polyP vs. DNA, alter the formation and behavior of enzymatic condensates.*

Following this comment, we investigated the phase separation behavior of CytR WT in the presence of different charge ratios of polyP-DNA mixtures. As seen in Author response image 1,panel A below, the outcomes are highly sensitive to the starting concentrations: at higher charge concentration of polyP (left panel), the OD and ThT fluorescence intensity is high at lower time points, both decrease and increase again. Fluorescence microscopy images (panel B) reveal similar trends, but the more fascinating outcome are the FRAP recovery profiles which recover extremely fast and fully at zero time point (panel C) despite aggregation-like tendencies observed in ThT fluorescence assays. However, at longer time points (20 and 40 mins) the FRAP recovery is significantly weaker but recovers to ~65% at 1 hour (panel C). At high relative polyP concentrations with respect to DNA, droplets are formed first which then transition into aggregates (liquid-to-solid transition; middle image in panel A). At relatively high DNA concentrations it appears that both droplets and aggregates co-exist as both OD and ThT fluorescence are moderately high. Given these complex behaviors, we have not included the same in the current manuscript as we still do not fully understand the origins of these differences. In fact, we are planning to extend this study by exploring the combinations in detail to understand the relative roles played by the two polymers in ternary mixtures.

Author response image 1.

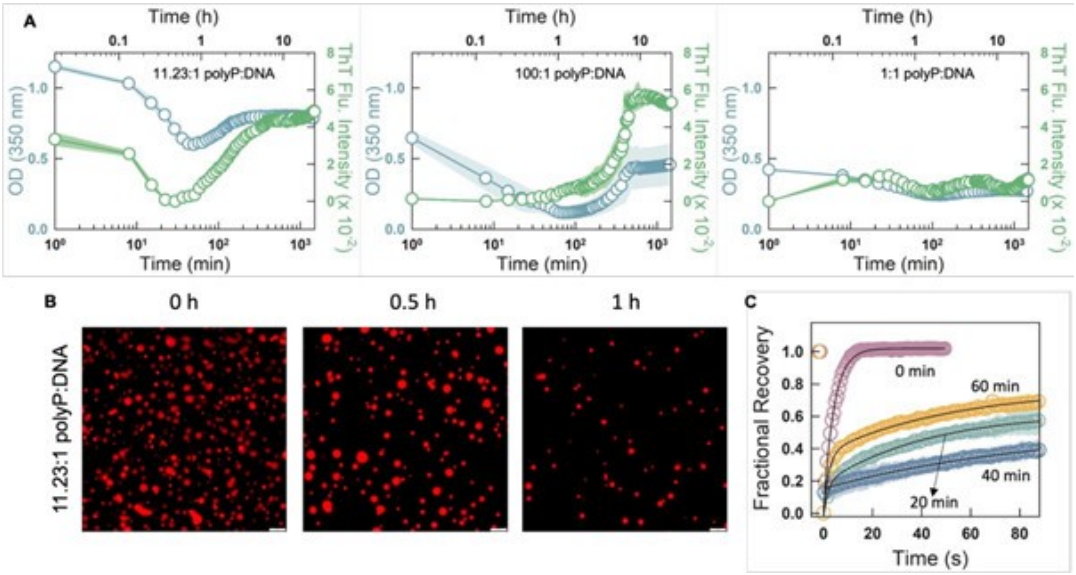

> *(3) In Figure 1H, the recovery trace shows the fractional recovery of DM to near WT levels. It is clear from the images that recovery of the bleached region occurs, but the overall fluorescence intensity of DM is much lower than WT, even when accounting for the difference in starting condensate sizes in the Pre-Bleach images. Shouldn't this qualitative difference in total fluorescence be reflected in the quantitative trace?*

In Figure 2H, as the reviewer rightly points out, there is a clear difference in the absolute fluorescence intensity between WT and DM condensates. We would like to clarify that the recovery traces shown in Figure 2I were normalized to the pre-bleach intensity of each individual condensate to reflect fractional recovery. This normalization is intended to highlight the relative mobility of the protein within each condensate, but it does not capture the difference in total fluorescence intensity between WT and DM.

> *(4) A description of the molten-globular variant Y19A FruR should be included in the main text where the variant is introduced. There is currently no additional description of the molten-globular variant in the Supplement as suggested by the manuscript.*

Figure 6A depicts the three-dimensional structure of FruR WT, with tyrosine residues Y19 and Y28, shown in red, forming stacking interactions. In the Y19A mutant, the loss of these interactions results in little changes in secondary structure (as shown in Figure 6E) but disrupts the protein's tertiary structure, resulting in a molten globular state. The FruR work is now published in JPCB and can be found at https://doi.org/10.1021/acs.jpcb.4c03895, and is also appropriately cited in the revised version (reference 53).

> *(5) Throughout the manuscript, the authors discuss polyP and DNA being able (or unable) to "distinguish" between different variants of CytR and FruR. This is confusing and suggests that DNA or polyP can choose to bind one form over another. The authors should re-work the language in this section to better reflect their direct observations for the behavior of protein in CD experiments and condensate behavior in imaging and turbidity experiments.*

We have now modified the text where necessary. The experiments were not done in the presence of both polyP and DNA, but in isolation (protein + polyP or protein + DNA). Hence, our aim is to convey that polyP is the polymer that leads to variable outcomes because of its ability to 'interact' differently with the different starting ensembles.

> *Minor Concerns:*
>
> *(1) For all Figures, please include the number of measurements, i.e., N = ...*

We have updated all figure legends to include the number of measurements, indicated as *N* = ..., as suggested.

> *(2) For all Figures, please place panel labels, i.e., A, B, C, etc., in the same respective location for each panel. As currently mapped out, it is difficult to easily determine which data are associated with each panel because the IDs are in various locations.*

Due to variations in data presentation and spacing within individual plots, it was challenging to place all labels in exactly the same position without obscuring important details. We have therefore maintained the labels as they were before.

> *(3) In the introduction, it would be helpful for the authors to specify exactly what is meant by chaperone. Given the context, it seems that the authors refer to the chaperone activity as one that prevents aggregation. Is this correct?*

We refer to chaperone activity specifically as the ability to prevent aggregation of proteins. We have now clarified this definition in the Introduction section of the revised manuscript.

> *(4) The results for experiments shown in Figure 3 need additional setup in the text. Were these measurements taken immediately after mixing WT, DM, or P33A with polyP? If so, why do condensates immediately appear and then dissipate before ThT-detected aggregates begin forming? Or were condensates allowed to form and then transferred to a different buffer, after which measurements were taken? Without a brief description of the experimental setup, interpreting the results is difficult.*

The condensates appear immediately after adding polyP to protein solutions, indicating that the condensate phase is kinetically accessible on mixing polyP with DM or the WT. As illustrated in Figure 3A and 3B, for WT protein, the condensates undergo liquid to solid transition over the time as this likely is the most thermodynamically stable phase. Effectively, this work is to convey that it is important to look at time-dependence of even droplets when formed as they may not be the most stable phase.

> *(5) Please include images of P33A over the time course of the experiment in Figure 3B.*

We have included the representative images of P33A in presence of polyP over the time in Figure 3B in the revised manuscript.

> *(6) In Figures 3D, E, G, and H, please plot each measurement separately with mean and standard deviation to enable the reader to see each data point.*

We have now revised Figures 3D, E, G, and H to show individual data points along with the mean and standard deviation.

> *(7) In the top paragraph on page 12, "fast-moving molecules" can be replaced with "dynamic molecules", as this offers a better description of the FRAP data.*

We have incorporated the suggested changes.

> *(8) In the "Structural changes within the condensates spans over three hours" results section on page 15, the conclusion reads "In summary, we find that both the WT and the DM 'unfold' on forming condensates with polyP..." The way this is written suggests that WT and DM behave in a similar manner. Given the CD data, however, it seems that by 4 hours, DM forms alpha helices while the WT does not. This suggests that while each unfolds, the conformation at 4 hours is different. The summary should reflect these differences.*

We fully agree with the reviewer on this. The summary is now modified to include the fact the DM forms alpha helices at 4 hours while the WT does not.

> *(9) At the end of the first paragraph of the results section "DNA does not discriminate the conformational ensembles" the authors should refer to Figure 2G, where they show the altered morphology of polP-P33A condensates.*

We have now included the reference to Figure 2G.

> *(10) The authors refer to droplets "solubilizing" throughout the manuscript. It seems that dissolve is a better term to use. Solubilize is better associated with individual biomolecules while dissolve is better associated with condensate behavior.*

We thank the reviewer for pointing this out. We have revised the manuscript to replace “solubilize” with “dissolve”.

> *(11) In Figures 5L and 5N, please change the Y-axis scale so that each curve is visible on the plot.*

We have adjusted the Y-axis scale in Figures 5L, 5M, and 5N to ensure that each curve is clearly visible and for easier comparison among the variants.

> *(12) The authors should show an image of FruR WT and Y19A with DNA for a direct comparison with experiments in which FruR and polyP were used. The addition of turbidity measurements of samples shown in Figure 6D will offer another direct comparison. As written, there is no way for the author to directly compare the effects of polyP and DNA on FruR phase transitions.*

As suggested, we have now included representative images of FruR WT and Y19A with DNA (Figure 6K and 6L) to enable a direct comparison with the FruR–polyP experiments. Also, we have already shown turbidity measurements in Figure 6B and 6C corresponding to the samples shown in Figure 6D.

> ***Reviewer 2:***
>
> *In this study, Goyal et al demonstrate that the assembly of proteins with polyphosphate into either condensates or aggregates can reveal information on the initial protein ensemble. They show that, unlike DNA, polyphosphate is able to effectively discriminate against initial protein ensembles with different conformational heterogeneity, structure, and compactness. The authors further show that the protein native ensemble is vital on whether polyphosphate induces phase separation or aggregation, whereas DNA induces a similar outcome regardless of the initial protein ensemble. This work provides a way to improve our mechanistic understanding of how conformational transitions of proteins*

> *may regulate or drive LLPS condensate and aggregate assemblies within biological systems.*

We thank the reviewer for the favorable comments on the manuscript.

> *Major Concerns:*
>
> *(1) The authors are using bacterial proteins (CytR and FruR) and solely represent polyphosphates as polyP45 (a polyphosphate with 45 Pi units). However, in bacterial systems, polyphosphates can be significantly longer (in the order of 100s to 1000 Pi units). Additionally, the experiments were run at neutral pH (7.0), and though this is fairly appropriate for the cytoplasm, volutin granules (where polyphosphates often accumulate) are typically considered slightly acidic (pH 5.5-6.5). From a physiological perspective, understanding how pH and the length of polyphosphate influence the ability to induce condensates or aggregates could be of importance.*

We appreciate the reviewer's insightful comments regarding the physiological relevance of polyphosphate length and pH. In our current study, we used polyP45 as it is easily available commercially and we conducted our experiments at pH 7 to mimic the general cytoplasm conditions. We agree that polyphosphates in bacterial cells can be significantly longer (hundreds to thousands of Pi units) and conducting experiments at slightly more acidic environment would be physiologically relevant. We plan to use longer polyP from Regene Tiss Inc. and acidic pH to explore how polyphosphate-induced phase separation of CytR vary with pH as a part of a future study. One could imagine doing all the experiments listed in the manuscript at different pH conditions for the different variants, but this could not be a part of the current work which has a specific focus on the differences in maturation properties depending on the nature of starting ensemble. However, the pKa values of the internal hydroxyl groups is ~2.2 (DOI:10.2147/IJN.S389819) indicating that the polyP carries near identical charges in the pH range between 4-7, and hence we expect little change in the charged status of polyP. On the other hand, the protonation states of charged amino acids within CytR could vary with pH, thus influencing its assembly properties.

> *(2) In the study, the longest metastable condensate induced by polyphosphate lasted approximately 3 hours before resolubilizing. It would be nice if the authors were able to generate a longer-lived condensate phase that would enable further mechanistic studies (e.g., NMR).*

We agree that generating longer-lived condensates would be highly valuable for mechanistic studies. However, the formation and stability of condensates is an intrinsic property of protein, and optimizing different conditions for a longer-lived condensate phase is beyond the scope of the current study. It is possible that the condensates are long-lived with longer polyP, but it is not clear if this would indeed be the case. We would also like to state here that while it is common to report on the liquid-to-solid transition in condensates, the intrinsic metastability of droplets (when there is no aggregation) is rarely reported. One possibility is to mutationally introduce cysteine residues and induce the formation of disulphide bridges (as done in a recent work, doi: 10.1021/jacs.4c09557) that make the condensate highly stable kinetically; however, this would also complicate the interpretation as the mechanism of condensate formation might be very different. We have therefore reported our results as an observation arising from differences in the nature of the poly-anionic polymers.

> *(3) The authors showed that CytR DM (fully folded), CytR WT (minor state folded), and CytR P33A (highly disordered) with polyphosphates lead to longer-lived condensates that resolubilize, shorterlived condensates that aggregate, and immediate aggregating, respectively. Whereas FruR (folded) and FruR Y19A (molten globular) with polyphosphate*

> *induce spontaneous aggregation and short-lived condensates, respectively. I would expect FruR to be more similar to CytR DM and FruR Y19A more similar to CytR WT in terms of structure and conformational dynamics and plasticity, yet they have opposing results. This raises a bit of concern. Meaning, that though polyphosphate discriminates between the different ensembles, is it actually possible to obtain information on the initial ensemble composition?*

In the current study, we show that CytR WT (less structured) and FruR Y19A (molten globule) form short-lived condensates that aggregate. We agree with the reviewer that while CytR DM (fully folded) forms condensates that dissolve over time, FruR WT (fully folded) variant forms aggregates immediately upon polyP addition. The observations show that polyP can discriminate between different protein conformations, in contrast to DNA, which does not show such selectivity. However, we acknowledge that while polyP-induced behavior reflects aspects of protein ensemble properties, it does not provide direct insight into the nature of the initial conformational ensemble.

> *(4) In the case of FruR with polyphosphate, no CD for the secondary structure analysis was provided as it was for CytR. It would be useful to see if the polyphosphate-induced structural changes observed for CytR hold true for FruR as well.*

We thank the reviewer for the suggestion. In response, we have performed far-UV CD experiments on FruR variants in the presence of polyP. Similar to the CytR WT, FruR WT shows unfolding upon polyP addition. A similar outcome is noted for the Y19A variant though there is significant residual helix content in the condensate unlike the WT. The CD spectra of FruR variants have been added to Figure 6.

> *Minor Concerns/Suggestions:*
>
> *Under conclusion, third paragraph, first sentence. This sentence reads, "Our observations thus establish that polyP efficiently discriminates the conformational features of proteins than DNA, contributing to the diverse outcomes."*

We thank the reviewer for pointing this out. The sentence has been revised for clarity. It now reads “Our observations establish that polyP is more sensitive to the conformational features of proteins than DNA, thereby contributing to the diverse outcomes.”

> *One experimental suggestion. Seeing that protein dynamics and plasticity seem to play a role. For either CytR WT or DM, it would be interesting to see the influence of temperature. Altering the temperature is a good way to perturb the population distribution of conformation sub-states and to alter kinetics. It may be that at a lower temperature (maybe 5C) for the WT you reduce conformational dynamics and you obtain results more similar to that of the DM. Alternatively, heating the DM would be another option. Obviously, there are additional challenges that may arise with changing the temperature, but if it were to work I think it could add some value.*

We thank the reviewer for the thoughtful suggestion. Due to limitations in our current experimental setup (as the reviewer notes as ‘challenges’)- the confocal set up does not have a temperature controller - we will not be to perform temperature-controlled assays. However, the ‘structure’ of CytR variants do not vary much between 280 – 298 K, and this is one of the reasons for choosing three variants without altering any other thermodynamic property. If temperature were varied, the dynamics of polyP would also change and hence the true molecule origins of any differences we might observe will be confounded by the dynamic effects on polyP as well. In this work, we have eliminated any dynamic differences in polyP by performing the experiments at a fixed temperature.

https://doi.org/10.7554/eLife.105461.2.sa0